

Role of postselection in generating vortex states of particles of arbitrary mass, spin, and energy

D. V. Karlovets,^{1,*} S. S. Baturin,¹ G. Geloni,² G. K. Sizykh,¹ and V. G. Serbo^{3,4,1}

¹*School of Physics and Engineering, ITMO University, 197101 St. Petersburg, Russia*

²*European XFEL, Holzkoppel 4, 22869 Schenefeld, Germany*

³*Novosibirsk State University, Pirogova 2, RUS-630090, Novosibirsk, Russia*

⁴*Sobolev Institute of Mathematics, Koptyuga 4, RUS-630090, Novosibirsk, Russia*

(Dated: August 31, 2022)

There exist many methods to obtain twisted photons with an orbital angular momentum up to the soft X-ray region. However, despite the big interest in generating massive particles with the phase vortices, the available diffraction techniques are only applicable to the moderately relativistic beams of electron microscopes, to cold neutrons, or to non-relativistic atoms. To bring matter waves physics into the high energy domain, one needs to develop alternative generation methods, applicable for ultrarelativistic energies and for composite particles. Here, we show that the vortex states of in principle arbitrary particles, including X- and γ -rays, muons, hadrons, nuclei, and ions, can be generated during photon emission in helical undulators, via Cherenkov radiation, in collisions of charged particles with intense laser beams, in such scattering or annihilation processes as $e\mu \rightarrow e\mu$, $ep \rightarrow ep$, $e^-e^+ \rightarrow p\bar{p}$, and so forth. We argue that the key element in obtaining them is the postselection protocol due to entanglement between a pair of final particles and it is largely not the process itself. The quantum state of a final particle – be it a photon, a proton, or a nucleus – becomes twisted if the azimuthal angle of the other particle momentum is measured with a large error or is not measured at all, which is often the case for small scattering angles. As a result, the requirements to the incoming beam transverse coherence can be greatly relaxed, which enables the generation of highly energetic vortex beams at accelerators and synchrotron radiation facilities, thus making them a new tool for hadronic and spin studies. This technique can also facilitate the development of sources of hard X-ray and γ -range twisted photons for nuclear and particle physics.

I. INTRODUCTION

Photons with a quantized projection of orbital angular momentum (OAM) onto a propagation axis were predicted in Ref.[1] and found numerous applications in quantum optics and quantum information, optomechanics, biology, astrophysics, and in other fields [2–9]. Along with the conventional diffraction techniques, such twisted states of light can be generated by charged particles during electromagnetic emission in helical undulators [10–15], via non-linear Thomson or Compton scattering [15–19] or – more generally – when the electron classical trajectory is helical [20, 21], during Cherenkov radiation and transition radiation in media with different characteristics [22, 23], and so forth. However, despite the proposals to use twisted photons in particle and nuclear studies [6], the highest energy of them achieved so far does not exceed but a few keV [7]. One recent idea to upconvert their frequency is to employ resonant scattering of the optical twisted photons on relativistic ions within the Gamma Factory project at the Large Hadron Collider [6, 24].

The massive counterparts of twisted photons – vortex electrons [25, 26] – were first generated in 2010-2011 with the 300 keV beams of transmission electron microscopes [27–29]. They have also attracted much attention outside the microscopy community because of their potential applications in atomic and high-energy physics [25, 26, 30–

50] and, in particular, in hadronic and spin studies (see the recent review [51]), and even in accelerator physics [52, 53] where classical analogues of the vortex packets – the so-called *angular-momentum-dominated beams* – have been utilized at accelerator facilities since the beginning of 2000s (see [54–56] and references therein).

There are ongoing discussions of possible experiments with other vortex particles, including elementary fermions heavier than electron, hadrons, ions and atoms, cold neutrons, nuclei, and even spin waves (magnons) [8, 34, 35, 41, 44–49, 52, 53, 57, 58]. Very recently, in 2021, the non-relativistic twisted atoms and molecules have been generated [59]. Clearly, a large class of quantum and classical waves can potentially carry phase vortices; however, the available diffraction techniques to generate such states [27–29, 60, 61] require the beams with high transverse coherence, typical for electron microscopes, and they are hardly applicable for relativistic beams of accelerators. This circumstance severely limits the development of the matter waves physics to higher energies.

Indeed, even if the beam current is low and there is no space-charge effect, the Rayleigh length of a relativistic electron packet does not exceed much the length of the collision region inside a linac, whereas in a storage ring or in an electromagnetic lens the rms-width $\sqrt{\langle \rho^2 \rangle}$ of a charged-particle wave packet does not grow but *oscillates* with time [53, 62–64], revealing the quantum betatron oscillations or broadening of the classical trajectories [65]. Therefore, the transverse coherence length of a quantum

* E-mail: d.karlovets@gmail.com

packet *naturally remains small*, and the corresponding dynamical effects do not usually play a role in collider experiments.

Thus, in order to boost the physics of vortex matter waves to the high-energy domain, we need to develop alternative methods to generate vortex states of a large class of quantum objects. Several such techniques based on the similarities between the quantum packets and the classical beams in accelerators have been recently discussed by one of us in [52, 53]. It was shown, in particular, that it is possible to accelerate charged particles with the phase vortices up to ultrarelativistic energies by modifying the particle sources.

In this paper, which is complementary to Ref.[66], we describe in detail a universal and versatile method to generate the vortex states of particles of in principle arbitrary mass, spin, and energy, including hard X-ray and γ -range twisted photons, relativistic muons, protons, ions and nuclei. Such particles can be obtained during emission of photons in electromagnetic fields of accelerators and free-electron lasers, via scattering or annihilation processes, such as

$$e\mu \rightarrow e\mu, ep \rightarrow ep, e^-e^+ \rightarrow h\bar{h}, e^-e^+ \rightarrow 2\gamma, \quad (1)$$

scattering of light on relativistic ions, which is being discussed within the Gamma Factory project at the LHC [6, 67], etc.

Our key observation is that it is largely *not the process itself* that defines whether a final particle gets a phase vortex or not, but a post-selection protocol due to entanglement between a pair of the final particles. Whereas in the classical theory the radiation field is always twisted if the emitting electron path is helical [20], the more general quantum theory developed in this paper predicts that the photons *cannot be twisted at all* if the emitting particle 3-momentum \mathbf{p}' is measured with a vanishing error, and that their OAM mostly depends on the way we post-select the emitting electron. When it comes to twisted photons, our results complement and specify those of the classical theory from Ref.[20], but also make them somewhat less optimistic because the conventional post-selection protocol, described, for instance, in the textbooks [68, 69], results in no vorticity of the emitted photons whatsoever.

We point out a deep analogy between a *generalized measurement* [70, 71] of a final particle momentum

$$\mathbf{p}' = \{p'_x, p'_y, p'_z\} = \{p'_\perp \cos \phi', p'_\perp \sin \phi', p'_z\}, \quad (2)$$

in which not all the components are measured with a vanishing error, and a standard von Neumann (projective) measurement in cylindrical basis [34], in which the momentum azimuthal angle $\phi' = \arctan(p'_y/p'_x)$ *does not belong to the measurable set* of quantum numbers. In more detail, if the azimuthal angle is measured with a very large error, this lack of information is enough for the evolved (pre-selected) state of the other final particle to become twisted, thanks to the entanglement and to the angle-OAM uncertainty relation [72, 73].

Thus, a crucial advantage of this generalized-measurements technique is that *neither modifications of the incoming beams are required nor there are any limitations* due to small transverse coherence of the beams. In a reaction with two final particles, to generate the vortex state of any particle – be it a photon, a neutron, a nucleus, or an ion – it is enough to measure the azimuthal angle of the other final particle with a large error or not to measure it at all. The proposed method can readily be employed for the generation of highly energetic vortex beams at the existing electron and hadron accelerators, X-ray free-electron lasers and synchrotron radiation facilities with helical undulators such as, for instance, the European XFEL and ESRF, powerful laser facilities such as the Extreme Light Infrastructure, and at the future linear colliders. A system of units with $\hbar = c = 1$ is used throughout the paper.

II. MEASUREMENT SCENARIOS

A. Evolved wave function of a particle

Let us consider emission of a photon by a charged particle (for definiteness, by an electron),

$$e \rightarrow e' + \gamma, \quad (3)$$

in the lowest order of the perturbation theory in QED. It can be Cherenkov radiation, synchrotron radiation, undulator radiation, transition radiation, and so on. A particle quantum state as it evolved after the reaction irrespectively of the measurement protocol can be called *pre-selected or evolved* because no measurement has been done yet. An initial state $|\text{in}\rangle$ of the electron and an evolved two-particle state of the final electron and the photon are connected via an evolution operator \hat{S} [68, 69],

$$|e', \gamma\rangle = \hat{S} |\text{in}\rangle = \sum_{\lambda_\gamma \lambda'} \int \frac{d^3 p'}{(2\pi)^3} \frac{d^3 k}{(2\pi)^3} S_{fi} |\mathbf{k}, \lambda_\gamma; \mathbf{p}', \lambda'\rangle, \quad (4)$$

where we have used the identity for the one-particle states (no virtual particles)

$$\sum_{\lambda_\gamma \lambda'} \int \frac{d^3 p'}{(2\pi)^3} \frac{d^3 k}{(2\pi)^3} |\mathbf{k}, \lambda_\gamma; \mathbf{p}', \lambda'\rangle \langle \mathbf{p}', \lambda'; \mathbf{k}, \lambda_\gamma| = \hat{1} \quad (5)$$

and

$$S_{fi} = \langle \mathbf{k}, \lambda_\gamma; \mathbf{p}', \lambda' | \hat{S} | \text{in} \rangle \quad (6)$$

is a matrix element with two final plane-wave states with the momenta \mathbf{p}' , \mathbf{k} and the helicities $\lambda' = \pm 1/2$, $\lambda_\gamma = \pm 1$. Without post-selection, the wave function of the evolved state is generally *not* factorized into a product of the photon wave function and that of the electron. Indeed, in the momentum representation we have

$$\langle \mathbf{p}', \mathbf{k} | e', \gamma \rangle = \sum_{\lambda_\gamma \lambda'} u' e S_{fi}, \quad (7)$$

where

$$\mathbf{e} \equiv \mathbf{e}_{\mathbf{k}\lambda_\gamma} \quad (8)$$

is a photon polarization vector in the Coulomb gauge, $\mathbf{e} \cdot \mathbf{k} = 0$, $\mathbf{e} \cdot \mathbf{e}^* = 1$, and

$$u' \equiv u_{p'\lambda'} \quad (9)$$

is a final electron bispinor, normalized as $\bar{u}'u' = 2m_e$ [68, 69]. So the final particles are generally *entangled*.

To derive the evolved wave function of the photon alone – that is, irrespectively of the photon detector – we need to disentangle the particles by post-selecting the electron. If it is post-selected to a state $|e'_{\text{det}}\rangle$, the photon wave function in momentum space becomes

$$\mathbf{A}^{(f)}(\mathbf{k}, \omega) = \sum_{\lambda_\gamma=\pm 1} \mathbf{e} S_{fi}, \quad (10)$$

where

$$S_{fi} = \langle \mathbf{k}, \lambda_\gamma; e'_{\text{det}} | \hat{S} | \text{in} \rangle. \quad (11)$$

This simple expression allows one to find in what quantum state the photon ends up as a result of the emission process itself, irrespectively of how this photon is detected afterwards, whereas the electron detected state is specified. The Fourier transform

$$\mathbf{A}^{(f)}(\mathbf{r}, \omega) = \int \frac{d^3\mathbf{k}}{(2\pi)^3} \mathbf{A}^{(f)}(\mathbf{k}, \omega) e^{i\mathbf{k}\cdot\mathbf{r}} \quad (12)$$

defines spatial distribution of the energy at the frequency ω in the Coulomb gauge, because $\mathbf{E}^{(f)}(\mathbf{r}, \omega) = i\omega\mathbf{A}^{(f)}(\mathbf{r}, \omega)$, and so

$$|\mathbf{E}^{(f)}(\mathbf{r}, \omega)|^2 = \omega^2 |\mathbf{A}^{(f)}(\mathbf{r}, \omega)|^2. \quad (13)$$

We emphasize the difference between this quantum picture and the classical theory: in the latter the electron path is given, the emitting particle experiences no recoil, the coherent properties and the phase of the radiation field are solely defined by the classical trajectory. In particular, when the electron path is circular or spiral the radiation field is always twisted [20]. The quantum picture *embraces the classical problem* as a special case (the Bohr correspondence principle), but it is inevitably more complex: the evolved state of the emitted photon itself always depends on how the emitting particle (electron) is post-selected. As we show below, if the electron 3-momentum is measured with the conventional plane-wave detector (the projective measurement), as it is in the overwhelming majority of experiments in particle physics [69], the final photon turns out to be *not twisted at all*, even if the electron wave-packet centroid moves along the helical path. Thus, the twisted particles are likely to be *not that abundant* in Nature as it follows from the classical theory.

Analogously, one can define an evolved (pre-selected) state of an electron, or of any other fermion, when the photon is post-selected to some state,

$$\psi^{(f)}(\mathbf{p}', \varepsilon') = \sum_{\lambda'=\pm 1/2} u' S_{fi}. \quad (14)$$

Clearly, the expressions (10), (14) also hold for scattering and annihilation processes, including reactions with hadrons in the final state. In the latter case, Eq.(14) can define an evolved wave function of the hadron.

B. Projective measurements in plane-wave basis

To begin with, let the initial electron be described as a plane-wave state propagating along the z axis with the momentum (say, in the problem of Cherenkov radiation below)

$$\mathbf{p} = \{0, 0, |\mathbf{p}|\}. \quad (15)$$

Following the conventional textbook approach [68, 69], if it is post-selected to a plane-wave state with the momentum $\mathbf{p}' = \{\mathbf{p}'_\perp, p'_z\}$ and the helicity λ' , the matrix element $S_{fi}^{(\text{pw})}$ and the photon's evolved wave function are both proportional to the momentum conservation delta-function

$$S_{fi}^{(\text{pw})} \propto \delta^{(3)}(\mathbf{p} - \mathbf{p}' - \mathbf{k}) \propto \delta^{(2)}(\mathbf{p}'_\perp + \mathbf{k}_\perp), \\ \mathbf{A}^{(f)}(\mathbf{k}, \omega) \propto \sum_{\lambda_\gamma=\pm 1} \mathbf{e} \delta(\mathbf{p}'_\perp + \mathbf{k}_\perp). \quad (16)$$

In other words, the projective measurements of the particle momenta with the vanishing errors are used in this scheme.

As soon as the azimuthal angle ϕ' of the electron momentum is precisely measured, the photon azimuthal angle ϕ_k is also set to a definite value

$$\phi_k = \phi' \pm \pi. \quad (17)$$

Thereby, the photon is projected to a plane-wave state *without* an intrinsic OAM projection on the z axis. One can qualitatively understand this result without the calculations by recalling the uncertainty relation from Ref.[72, 73]: *a definite azimuthal angle of a plane wave implies a vanishing mean OAM z -projection but an infinitely wide OAM spectrum* (see appendix A for more detail).

Now let us take a general reaction with the plane-wave states, the matrix element of which is proportional to the energy-momentum conservation delta-function [68, 69],

$$S_{fi}^{(\text{pw})} \propto \delta^{(4)}(\sum p_{\text{in}} - \sum p_{\text{out}}). \quad (18)$$

If we substitute this to Eq.(10) or Eq.(14), we immediately see that the evolved wave function of a photon or of a fermion has a well-defined 4-momentum, which automatically means that the z projection of the intrinsic OAM is vanishing.

The post-selection to the plane waves or projective measurements in the plane-wave basis is the most frequently used approach both in calculations and in experiments on particle scattering, annihilation, or photon emission. As we have already said, in quantum theory it

is not the particle trajectory but the post-selection protocol that defines vorticity of the final photon. Therefore, when it comes to the photon phase, direct comparison of the results in the plane-wave basis with the classical theory simply *does not have sense*. Indeed, the classical electron does not experience recoil, so its angle ϕ' is not defined, which is more similar to the generalized-measurement scheme (iii) below than to the above projective measurement approach.

C. Cylindrical basis and generalized measurements

The post-selection to a plane wave represents a projective measurement when all components of the momentum \mathbf{p}' (see Eq.(2)) are measured with vanishing errors. During a generalized measurement, on the contrary, at least some of the components are measured with a *non-vanishing* error (see, e.g., [70, 71]). If the error of some component is maximal, we do not effectively measure this component at all. Put simply, a generalized measurement is a post-selection to a wave packet, a coherent superposition of plane waves,

$$|e'_{\text{det}}\rangle^{(\text{g})} = \int \frac{d^3 p'}{(2\pi)^3} \psi(\mathbf{p}') |\mathbf{p}', \lambda'\rangle, \quad (19)$$

where the overlap function $\psi(\mathbf{p}')$ is normalized. The set of operators

$$|e'_{\text{det}}\rangle^{(\text{g})} \langle e'_{\text{det}}|^{(\text{g})} \quad (20)$$

is complete, although *not necessarily orthogonal*, and it forms a positive operator-valued measure [70].

There exists a close relative of the generalized measurement, called *the weak measurement* [74–77], during which an observable quantity is also measured with a finite error, but the measured *weak values* do not necessarily belong to the spectrum of the corresponding operator and they can even be complex. The operators (20), needed for our purposes, are hermitian and positively-defined, so the measured values of the azimuthal angle below still belong to the interval $[0, 2\pi]$, which is why we adhere to the term “generalized measurement” in what follows.

The overlap function can be of the Gaussian form,

$$\psi(\mathbf{p}') \propto \prod_i \exp \left\{ -(p'_i - \langle p_i \rangle)^2 / (2\sigma_i)^2 \right\}. \quad (21)$$

where $i = x, y, z$ or $i = \rho, \phi, z$. A projective measurement implies that

$$\sigma_x, \sigma_y, \sigma_z \rightarrow 0. \quad (22)$$

Alternatively, one can use the cylindrical coordinates $p'_\perp, \phi' = \arctan(p'_y/p'_x), p'_z$ with the corresponding uncertainties $\sigma_\perp, \sigma_\phi, \sigma_z$. For a generalized measurement, at least one of these uncertainties is not vanishing.

To provide completeness of the set (20), one generally needs to measure both the non-commutative observables, the simplest example being the coordinates and

momenta. The corresponding normalized wave packet can be written as (we omit the helicity sign for now)

$$\begin{aligned} |e'_{\text{det}}\rangle^{(\text{g})} &= |\langle \mathbf{r} \rangle, \langle \mathbf{p} \rangle\rangle = \\ &= \int \frac{d^3 p'}{(2\pi)^3} \prod_i \frac{(2\pi)^{3/2}}{(2\pi\sigma_i^2)^{1/4}} e^{-\frac{(p'_i - \langle p_i \rangle)^2}{(2\sigma_i)^2} - i\langle \mathbf{r} \rangle \cdot \mathbf{p}'} |\mathbf{p}'\rangle, \\ &\langle \langle \mathbf{r} \rangle, \langle \mathbf{p} \rangle | \langle \mathbf{r} \rangle, \langle \mathbf{p} \rangle \rangle = 1, \\ &\langle \langle \mathbf{r} \rangle, \langle \mathbf{p} \rangle | \hat{\mathbf{p}} | \langle \mathbf{r} \rangle, \langle \mathbf{p} \rangle \rangle = \langle \mathbf{p} \rangle, \\ &\langle \langle \mathbf{r} \rangle, \langle \mathbf{p} \rangle | \hat{\mathbf{x}} | \langle \mathbf{r} \rangle, \langle \mathbf{p} \rangle \rangle = \langle \mathbf{r} \rangle, \end{aligned} \quad (23)$$

and this set is complete

$$\begin{aligned} \int d^3 \langle \mathbf{r} \rangle \frac{d^3 \langle \mathbf{p} \rangle}{(2\pi)^3} |\langle \mathbf{r} \rangle, \langle \mathbf{p} \rangle\rangle \langle \langle \mathbf{r} \rangle, \langle \mathbf{p} \rangle| &= \\ = \int \frac{d^3 p'}{(2\pi)^3} |\mathbf{p}'\rangle \langle \mathbf{p}'| &= \hat{1}. \end{aligned} \quad (24)$$

Note that this feature only invokes the completeness of the momentum eigenstates, but not of the coordinate eigenstates, which is natural for relativistic theory. These packets represent the so-called *coherent states* of a freely propagating massive particle [78].

To illustrate these ideas, let us distinguish the following three scenarios (see Fig.1):

(i) We post-select the particles to the plane-wave states and repeat the measurements many times with an ensemble of electrons, each time fixing the detector at a different angle ϕ' . The emission rate or a cross section are proportional to

$$\int_0^{2\pi} \frac{d\phi'}{2\pi} |S_{fi}^{(\text{pw})}|^2, \quad (25)$$

which represents *an incoherent* averaging over the azimuthal angle in the projective-measurement scheme. This is the standard textbook approach with the projective measurements [68, 69], in which no phases contribute to the observable quantities.

(ii) Another example of a projective measurement is post-selection to a cylindrical wave (a Bessel state) [34] with the definite p'_\perp, p'_z , the z -projection of *the total angular momentum* (TAM) m' , and the helicity λ' , but undefined angle ϕ'

$$\begin{aligned} |e'_{\text{det}}\rangle &= |p'_\perp, p'_z, m', \lambda'\rangle = \\ &= \int_0^{2\pi} \frac{d\phi'}{2\pi} i^{-(m' - \lambda')} e^{i(m' - \lambda')\phi'} |\mathbf{p}', \lambda'\rangle. \end{aligned} \quad (26)$$

The TAM z -projection operator

$$\hat{j}_z |p'_\perp, p'_z, m', \lambda'\rangle = m' |p'_\perp, p'_z, m', \lambda'\rangle, \quad (27)$$

is a sum of an orbital part \hat{L}_z and a spin part \hat{s}_z . The former is

$$\hat{L}_z = [\hat{\mathbf{r}} \times \hat{\mathbf{p}}]_z = -i \frac{\partial}{\partial \phi}, \quad (28)$$

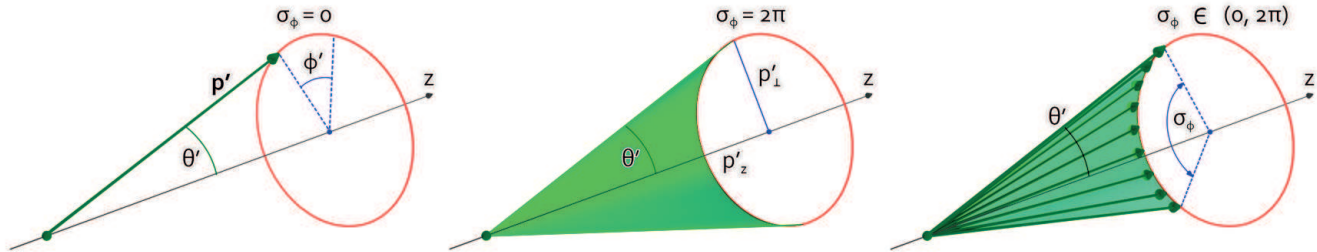


FIG. 1. The possible measurement strategies. Left: the conventional plane-wave approach (i) (projective measurement) with the definite 3-momentum \mathbf{p}' , middle: the projective measurement in the cylindrical basis (ii) with an undefined azimuthal angle ϕ' of the momentum, right: the generalized-measurement scheme (iii) with a finite uncertainty σ_ϕ of the azimuthal angle. In all three scenarios, the states are stationary with the definite energy, $\varepsilon' = \sqrt{(p'_\perp)^2 + (p'_z)^2 + m_e^2}$.

while the latter depends on the particle spin. Here, ϕ refers to the azimuthal angle either of \mathbf{r} or of \mathbf{p} , depending on the representation.

The corresponding amplitude

$$\int_0^{2\pi} \frac{d\phi'}{2\pi} i^{-(m'-\lambda')} e^{i(m'-\lambda')\phi'} S_{fi}^{(\text{pw})} \quad (29)$$

represents a *coherent* averaging over the azimuthal angle, whereas the detector is able to measure the TAM with a vanishing error $\sigma_m \rightarrow 0$. As the azimuthal angle and the z -projection of the angular momentum represent *the conjugate variables* [72], in this way we also obtain the complete information about the electron, but in the cylindrical basis.

(iii) Consider now an electron emitting a photon in the case we measure the azimuthal angle ϕ' of the final electron momentum with a finite error (see the right panel in Fig.1)

$$\sigma_\phi \in (0, 2\pi). \quad (30)$$

Generally, in this scheme we post-select to the wave packet (19) with the finite uncertainties $\sigma_\perp, \sigma_\phi, \sigma_z$. The finite uncertainty σ_ϕ means that we do not know exactly at which azimuthal angle the final electron goes, and the maximal value, $\sigma_\phi \rightarrow 2\pi$, corresponds to a special case when the angle is not known at all or, simply, is not measured. The corresponding uncertainty relation [72] says that the larger the error of the angle is, the smaller the corresponding OAM error.

If $\sigma_\phi \rightarrow 2\pi$, the information about the electron momentum is *incomplete*, but the energy is well-defined,

$$\varepsilon' = \sqrt{(p'_\perp)^2 + (p'_z)^2 + m_e^2}. \quad (31)$$

The corresponding amplitude is also obtained via the co-

herent averaging,

$$\int_0^{2\pi} \frac{d\phi'}{2\pi} S_{fi}^{(\text{pw})}. \quad (32)$$

Formally, this expression coincides with (29) at $m' - \lambda' = 0$, but its physical meaning is different. In the projective-measurement scheme (ii), we do measure the TAM projection and the helicity, and we can easily obtain $\langle \hat{L}_z \rangle = m' - \lambda' = 0$, but during the generalized measurement we may not effectively measure the TAM at all when the error is maximized, which implies projection to the state

$$|e'_{\text{det}}\rangle^{(\text{g})} = \int_0^{2\pi} \frac{d\phi'}{2\pi} |\mathbf{p}', \lambda'\rangle, \quad (33)$$

where each plane wave enters with the same phase. The corresponding function $\psi(\mathbf{p}')$ from Eq.(19)

$$\psi(\mathbf{p}') = (2\pi)^2 \delta(p'_z - \langle p \rangle_z) \frac{1}{p'_\perp} \delta(p'_\perp - \langle p \rangle_\perp) \quad (34)$$

does not depend on the angle ϕ' .

Returning to the formula (23) for the normalized wave packet, we note that whereas the delta functions in Eq.(34) can be obtained as the special cases of the Gaussian envelopes, the term $\exp\{-i\langle \mathbf{r} \rangle \cdot \mathbf{p}'\}$ is absent here. Indeed, in the wave-packet approach we also measure the conjugate variables, that is the mean path $\langle \mathbf{r} \rangle$ of the packet at the same moment of time (if we choose this to be $t = 0$, then $\langle \mathbf{r} \rangle$ has a sense of the initial conditions). As we do not measure the momentum azimuthal angle now, the mean components of the transverse momentum are vanishing, $\langle p_x \rangle = \langle p_y \rangle = 0$, exactly as they are in the scheme (ii) with the Bessel beams. So the mean path of the final packet should be taken as $\langle \mathbf{r} \rangle = \{0, 0, \langle z \rangle\}$, even though $\langle \mathbf{p}_\perp^2 \rangle = \langle p_x^2 \rangle + \langle p_y^2 \rangle \neq 0$, which is why we can safely omit the term $\exp\{-i\langle \mathbf{r} \rangle \cdot \mathbf{p}'\} = \exp\{-i\langle z \rangle p'_z\}$ in Eq.(34).

The expansion reverse to Eq.(26) is (see appendix A)

$$|\mathbf{p}', \lambda'\rangle = \sum_{m'-\lambda'=-\infty}^{\infty} i^{m'-\lambda'} e^{-i(m'-\lambda')\phi'} |p'_{\perp}, p'_z, m', \lambda'\rangle. \quad (35)$$

Therefore one can look at the scheme (iii) as at an averaging over the phase space during the projective measurement in the cylindrical basis (scheme (ii)),

$$|e'_{\text{det}}\rangle^{(g)} = \int_0^{2\pi} \frac{d\phi'}{2\pi} \times \sum_{m'-\lambda'=-\infty}^{\infty} i^{m'-\lambda'} e^{-i(m'-\lambda')\phi'} |p'_{\perp}, p'_z, m', \lambda'\rangle, \quad (36)$$

where the probability to get a definite TAM m' during

$$\delta(\mathbf{p}'_{\perp} + \mathbf{k}_{\perp}) = \delta(p'_x + k_x)\delta(p'_y + k_y) = \frac{1}{p'_{\perp}} \delta(p'_{\perp} - k_{\perp}) \left(\delta(\phi' - (\phi_k - \pi)) \Big|_{\phi_k \in [\pi, 2\pi]} + \delta(\phi' - (\phi_k + \pi)) \Big|_{\phi_k \in [0, \pi]} \right). \quad (39)$$

Note that only one of these configurations contributes to the evolved state, and there is no interference between them (cf. Ref.[8, 40, 45]).

So, in the simplest generalized-measurement scheme with $\sigma_{\phi} \rightarrow 2\pi$ the evolved wave functions of the photon and of the fermion, Eq. (10) and Eq.(14), become

$$\begin{aligned} \mathbf{A}_{(g)}^{(f)}(\mathbf{k}, \omega) &= \sum_{\lambda_{\gamma}=\pm 1} e \int_0^{2\pi} \frac{d\phi'}{2\pi} S_{fi}^{(\text{pw})} \propto \\ &\propto \int \frac{d\phi'}{2\pi} \delta(\mathbf{p}'_{\perp} + \mathbf{k}_{\perp}) \propto \frac{1}{p'_{\perp}} \delta(p'_{\perp} - k_{\perp}), \\ \psi_{(g)}^{(f)}(\mathbf{p}', \varepsilon') &= \sum_{\lambda'=\pm 1/2} u' \int_0^{2\pi} \frac{d\phi'}{2\pi} S_{fi}^{(\text{pw})}. \end{aligned} \quad (40)$$

where for the fermion the integration is performed over the azimuthal angle of the particle measured in the generalized scheme. The proportionality to $\delta(\mathbf{p}'_{\perp} - \mathbf{k}_{\perp})$ instead of $\delta(\mathbf{p}'_{\perp} + \mathbf{k}_{\perp})$ is a hallmark of the Bessel state with the definite TAM z-projection and its vanishing uncertainty.

The generalized measurement scheme with the finite uncertainty $0 < \sigma_{\phi} < 2\pi$ employs a function $g(\phi, \sigma_{\phi})$, and so

$$\begin{aligned} \mathbf{A}_{(g)}^{(f)}(\mathbf{k}, \omega) &= \sum_{\lambda_{\gamma}=\pm 1} e \int_0^{2\pi} \frac{d\phi'}{2\pi} g(\phi', \sigma_{\phi}) S_{fi}^{(\text{pw})}, \\ \psi_{(g)}^{(f)}(\mathbf{p}', \varepsilon') &= \sum_{\lambda'=\pm 1/2} u' \int_0^{2\pi} \frac{d\phi'}{2\pi} g(\phi', \sigma_{\phi}) S_{fi}^{(\text{pw})}. \end{aligned} \quad (41)$$

where $g(\phi', 0) = \delta(\phi' - \tilde{\phi}')$ and $g(\phi', 2\pi) = 1$. In particular, when $|\sigma_{\phi} - 2\pi| \ll 2\pi$, the function g is smooth. Clearly, the latter case describes a Bessel-like wave packet

the projective measurement,

$$|i^{m'-\lambda'} e^{-i(m'-\lambda')\phi'}|^2 = 1, \quad (37)$$

is the same for all $m' - \lambda'$. The measure

$$\int \frac{d\phi'}{2\pi} \sum_{m'-\lambda'=-\infty}^{\infty} \quad (38)$$

is a total number of the mutually orthogonal states in the particle phase space, which is obviously infinite for the delocalized cylindrical waves.

Working in cylindrical coordinates, we use the following representation for the delta-function of the transverse momentum conservation (see Fig.2):

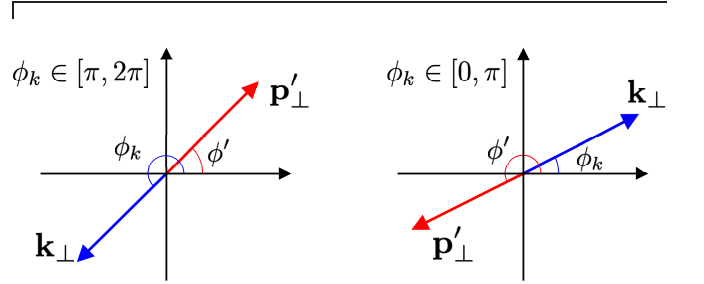


FIG. 2. Two possible directions of the vectors \mathbf{k}_{\perp} and \mathbf{p}'_{\perp} according to Eq.(39).

with a mean TAM z-projection $\langle \hat{j}_z \rangle$ and a *finite* TAM uncertainty, $\Delta j_z \ll \langle \hat{j}_z \rangle$. In what follows, we discuss the scheme with $\sigma_{\phi} \rightarrow 2\pi$ for simplicity.

Importantly, the different measurement protocol does not alter the total number of particles produced in a specific reaction. Finally, note that this generalized-measurement scenario can, somewhat surprisingly, guarantee the validity of the *Bohr correspondence principle* in the quasi-classical regime of electromagnetic emission when the emitting particle experiences very small recoil and the scattering angle is vanishing, $\theta' \ll 1$. For instance, in a number of scattering and emission processes, including Cherenkov radiation, synchrotron radiation, and the Compton effect, this angle is of the order of

$$\theta' \sim 10^{-6} - 10^{-5} \text{ rad} \quad (42)$$

for electrons and realistic parameters. Therefore, precise measurements of the azimuthal angle ϕ' can technically be *very challenging* at these small polar angles. This is the reason why predictions of this genuinely

quantum generalized-measurement scheme provide coincidence with the classical theory.

III. WORKING IN THE TAM BASIS

In the conventional plane-wave approach (*i*), the observable emission rates or the cross sections do not depend on the wave functions phases. Here, we are interested in phases of the evolved wave functions, which is why an analysis of the general phases of the electron bispinors is needed before coming to examples.

A. When phases matter

A two-component spinor $w^{(\lambda)}(\theta, \phi) \equiv w^{(\lambda)}$ – an eigenstate of the helicity operator $\hat{\mathbf{s}} \cdot \mathbf{p}/|\mathbf{p}|$ – can be expanded into a series over the eigenstates of the \hat{s}_z operator,

$$\begin{aligned} w^{(\lambda)} &= \sum_{\sigma=\pm 1/2} w^{(\sigma)} d_{\sigma\lambda}^{(1/2)}(\theta) e^{-i(\sigma-\lambda)\phi}, \\ w^{(\sigma=1/2)} &= (1, 0)^T, \quad w^{(\sigma=-1/2)} = (0, 1)^T, \\ \hat{s}_z w^{(\sigma)} &= \sigma w^{(\sigma)}, \quad \hat{j}_z w^{(\lambda)} = \lambda w^{(\lambda)}, \end{aligned} \quad (43)$$

and θ is the momentum polar angle, $p_\perp = |\mathbf{p}| \sin \theta$, $p_z = |\mathbf{p}| \cos \theta$. The functions

$$d_{\sigma\lambda}^{(1/2)}(\theta) = \delta_{\sigma\lambda} \cos(\theta/2) - 2\sigma \delta_{\sigma,-\lambda} \sin(\theta/2) \quad (44)$$

are sometimes called the small Wigner functions and described, for instance, in Ref.[87].

The choice of the overall phase of the spinor $w^{(\lambda)}$ defines the eigenvalue of the \hat{j}_z operator. The above phase $e^{i\lambda\phi}$ corresponds to the eigenvalue λ of the TAM operator and without this phase the eigenvalue would be vanishing, $\hat{j}_z w^{(\lambda)} = 0$. The latter choice is made in the textbook [68], where the Dirac electron bispinor $\tilde{u}_{p\lambda}$, also a helicity state, looks as follows:

$$\begin{aligned} \tilde{u}_{p\lambda} &\equiv \sum_{\sigma=\pm 1/2} u_{\varepsilon\lambda}^{(\sigma)} d_{\sigma\lambda}^{(1/2)}(\theta) e^{-i\sigma\phi}, \\ u_{\varepsilon\lambda}^{(\sigma)} &= (\sqrt{\varepsilon + m_e} w^{(\sigma)}, 2\lambda \sqrt{\varepsilon - m_e} w^{(\sigma)})^T, \\ \hat{s}_z u_{\varepsilon\lambda}^{(\sigma)} &= \sigma u_{\varepsilon\lambda}^{(\sigma)}, \quad \hat{j}_z \tilde{u}_{p,\lambda} = 0, \end{aligned} \quad (45)$$

Clearly, the operator $\hat{j}_z = \hat{s}_z + \hat{L}_z$ commutes with the Dirac Hamiltonian, so its eigenvalue is a conserved quantum number.

The phase $e^{i\lambda\phi}$ in Eq.(43) yields the same general phase of the bispinor $u_{p\lambda}$, which changes the orbital part and shifts the TAM to a non-vanishing value,

$$\begin{aligned} \tilde{u}_{p\lambda} e^{i\lambda\phi} &\rightarrow u_{p\lambda}, \\ u_{p\lambda} &\equiv \sum_{\sigma=\pm 1/2} u_{\varepsilon\lambda}^{(\sigma)} d_{\sigma\lambda}^{(1/2)}(\theta) e^{-i(\sigma-\lambda)\phi}, \\ \hat{j}_z u_{p\lambda} &= \lambda u_{p\lambda}. \end{aligned} \quad (46)$$

Such a choice of the phase is made in the textbook [69].

The difference between the two choices is clearly seen when the z axis is chosen along the momentum \mathbf{p} , $\theta \rightarrow$

0. The state (45) with $\langle j_z \rangle = 0$ still depends on the azimuthal angle ϕ

$$w^{(\lambda)}(\theta \rightarrow 0, \phi) \rightarrow w^{(\sigma)} e^{-i\sigma\phi}, \quad (47)$$

which is somewhat unnatural because it leads to a non-vanishing OAM. The state with $\langle j_z \rangle = \lambda$ does not have this phase factor. In what follows, we denote as $\tilde{u}_{p\lambda}$ the bispinors with a vanishing TAM projection (the choice of [68]), while we keep $u_{p\lambda}$ for the bispinor with the TAM projection $\langle j_z \rangle = \lambda$ (the choice of [69]). The corresponding short-hand notations are

$$\tilde{u}_{p\lambda} \equiv \tilde{u} \quad \text{and} \quad u_{p\lambda} \equiv u, \quad (48)$$

respectively. So, whereas the overall phases are *not* relevant during the projective measurements, for which the probability depends on $|S_{fi}^{(pw)}|^2$, the phases can become important in the generalized-measurement scheme.

B. Transition current

When calculating the matrix elements in the head-on geometry, we deal with the transition currents in momentum space. Let us calculate the current between two free fermions with the mass m_e , the energies ε and ε' , and with the definite TAM z -projections λ and λ' . Let the initial fermion propagate along the z axis, $\mathbf{p} = \{0, 0, |\mathbf{p}|\}$, the angles of the final fermion are θ', ϕ' . By using the above formulas we get

$$\begin{aligned} \bar{u}_{p'\lambda'} \gamma^\mu u_{p\lambda} &= J^\mu e^{i(\lambda-\lambda')\phi'}, \\ J^\mu &= \{J^0, \mathbf{J}\}, \\ J^0 &= d_{\lambda\lambda'}^{(1/2)}(\theta') \left(\sqrt{\varepsilon + m_e} \sqrt{\varepsilon' + m_e} + \right. \\ &\quad \left. + 2\lambda 2\lambda' \sqrt{\varepsilon - m_e} \sqrt{\varepsilon' - m_e} \right), \\ \mathbf{J} &= (\sqrt{\varepsilon' + m_e} \sqrt{\varepsilon - m_e} + 2\lambda 2\lambda' \sqrt{\varepsilon + m_e} \sqrt{\varepsilon' - m_e}) \\ &\quad \times \left(d_{\lambda\lambda'}^{(1/2)}(\theta') \boldsymbol{\chi}_0 - \sqrt{2} d_{-\lambda\lambda'}^{(1/2)}(\theta') \boldsymbol{\chi}_{2\lambda} e^{-i2\lambda\phi'} \right), \end{aligned} \quad (49)$$

where γ^μ are the 4×4 Dirac matrices in the standard representation [68] and

$$\begin{aligned} \boldsymbol{\chi}_0 &= (0, 0, 1)^T, \quad \boldsymbol{\chi}_{\pm 1} = \mp \frac{1}{\sqrt{2}} (1, \pm i, 0)^T, \\ \boldsymbol{\chi}_\Lambda^\dagger \cdot \boldsymbol{\chi}_{\Lambda'} &= \delta_{\Lambda\Lambda'}, \\ \hat{s}_z \boldsymbol{\chi}_\Lambda &= i \boldsymbol{\chi}_0 \times \boldsymbol{\chi}_\Lambda = \Lambda \boldsymbol{\chi}_\Lambda, \quad \Lambda = 0, \pm 1. \end{aligned} \quad (50)$$

Here, \hat{s}_z is a photon spin operator. We have also used the equality

$$\begin{aligned} (w^{(\sigma')})^\dagger \{1, \boldsymbol{\sigma}\} w^{(\sigma)} &= \\ = \{ \delta_{\sigma\sigma'}, 2\sigma (\boldsymbol{\chi}_0 \delta_{\sigma,\sigma'} - \sqrt{2} \delta_{\sigma,-\sigma'} \boldsymbol{\chi}_{2\sigma}) \}, \end{aligned} \quad (51)$$

where $\boldsymbol{\sigma}$ are the Pauli matrices. Note that J^0 does not depend on ϕ' .

Likewise, we can calculate the current when the initial particle propagates opposite to the z axis,

$$\mathbf{p} = \{0, 0, -|\mathbf{p}|\}. \quad (52)$$

We denote the corresponding spinors of the incoming particle as $u_{p\lambda}(-\mathbf{p})$ and $\omega^{(\lambda)}(-\mathbf{p})$. We arrive at

$$\begin{aligned} \bar{u}_{p'\lambda'}\gamma^\mu u_{p\lambda}(-\mathbf{p}) &= J^\mu(-\mathbf{p})e^{-i(\lambda+\lambda')\phi'}, \\ J^0(-\mathbf{p}) &= d_{-\lambda\lambda'}^{(1/2)}(\theta') \left(\sqrt{\varepsilon+m_e}\sqrt{\varepsilon'+m_e} + \right. \\ &\quad \left. + 2\lambda 2\lambda'\sqrt{\varepsilon-m_e}\sqrt{\varepsilon'-m_e} \right), \\ \mathbf{J}(-\mathbf{p}) &= \left(\sqrt{\varepsilon'+m_e}\sqrt{\varepsilon-m_e} + 2\lambda 2\lambda'\sqrt{\varepsilon+m_e}\sqrt{\varepsilon'-m_e} \right) \\ &\quad \times \left(-d_{-\lambda\lambda'}^{(1/2)}(\theta')\boldsymbol{\chi}_0 + \sqrt{2}d_{\lambda\lambda'}^{(1/2)}(\theta')\boldsymbol{\chi}_{-2\lambda} e^{i2\lambda\phi'} \right). \end{aligned} \quad (53)$$

Importantly, $u_{p\lambda}(-\mathbf{p}) \neq u_{p,-\lambda}$, but $\omega^{(\lambda)}(-\mathbf{p}) = \omega^{(-\lambda)}$, and the latter transition current cannot be obtained from Eq.(49) by simply swapping $\lambda \rightarrow -\lambda$. Now we are ready to give some examples.

IV. EXAMPLE 1: CHERENKOV RADIATION

Consider Cherenkov radiation,

$$e(p) \rightarrow e'(p') + \gamma(k), \quad (54)$$

in a transparent medium with weak frequency dispersion and a refractive index $n(\omega)$; see Fig.3. The incoming electron is described as a plane wave and the matrix element is

$$S_{fi}^{(pw)} = -ieN(2\pi)^4\delta^{(4)}(p-p'-k)\bar{u}'\gamma^\mu u e_\mu^*, \quad (55)$$

where N is a normalization constant and

$$\begin{aligned} p &= \{\varepsilon, 0, 0, |\mathbf{p}|\}, \quad p' = \{\varepsilon', p'_\perp \cos \phi', p'_\perp \sin \phi', p'_z\}, \\ p'_\perp &= |\mathbf{p}'| \sin \theta', \quad k = \{\omega, k_\perp \cos \phi_k, k_\perp \sin \phi_k, k_z\}, \\ |\mathbf{k}| &= \sqrt{k_\perp^2 + k_z^2} = \omega n(\omega), \quad k_\perp = |\mathbf{k}| \sin \theta_k. \end{aligned} \quad (56)$$

The phases are chosen so that the electron bispinors are eigenfunctions of the TAM z-projection operator with the eigenvalues $\lambda = \pm 1/2, \lambda' = \pm 1/2$.

If the electron is detected in the above generalized-measurement scheme, we do not know the photon momentum azimuthal angle. Then, the photon evolved state is (see Eq.(10))

$$\begin{aligned} \mathbf{A}^{(f)}(\mathbf{k}, \omega) &= \int_0^{2\pi} \frac{d\phi'}{2\pi} \sum_{\lambda_\gamma=\pm 1} e S_{fi}^{(pw)} = -ieN \times \\ &\quad \times \mathbf{n} \times \left[\mathbf{n} \times \int_0^{2\pi} \frac{d\phi'}{2\pi} (2\pi)^4 \delta^{(4)}(p-p'-k) \bar{u}'\gamma u \right], \end{aligned} \quad (57)$$

where $\mathbf{n} = \mathbf{k}/|\mathbf{k}|$, we employ the Coulomb gauge with $e^\mu = \{0, \mathbf{e}\}$, and the summation over the photon helicities is done with the following formula

$$\sum_{\lambda_\gamma=\pm 1} e_i e_j^* = \delta_{ij} - n_i n_j. \quad (58)$$

Substituting Eq.(39) to Eq.(57), we arrive at

$$\begin{aligned} \mathbf{A}^{(f)} &= (-1)^{\lambda-\lambda'} ieN(2\pi)^3 \delta(\varepsilon-\varepsilon'-\omega) \delta(|\mathbf{p}|-p'_z-k_z) \frac{1}{p'_\perp} \delta(p'_\perp-k_\perp) \\ &\quad \times \left(\sqrt{\varepsilon'+m_e}\sqrt{\varepsilon-m_e} + 2\lambda 2\lambda'\sqrt{\varepsilon+m_e}\sqrt{\varepsilon'-m_e} \right) [\mathbf{F} - \mathbf{n}(\mathbf{nF})], \end{aligned} \quad (59)$$

where

$$\begin{aligned} \mathbf{F} &= d_{\lambda\lambda'}^{(1/2)}(\theta') \boldsymbol{\chi}_0 e^{i(\lambda-\lambda')\phi_k} + \\ &\quad + \sqrt{2} d_{-\lambda\lambda'}^{(1/2)}(\theta') \boldsymbol{\chi}_{2\lambda} e^{-i(\lambda+\lambda')\phi_k}. \end{aligned} \quad (60)$$

Thus, the two terms with $\boldsymbol{\chi}_0 e^{i(\lambda-\lambda')\phi_k}$ and $\boldsymbol{\chi}_{2\lambda} e^{-i(\lambda+\lambda')\phi_k}$ in \mathbf{F} are eigenvectors of \hat{s}_z operator with the eigenvalues 0 and 2λ , respectively, and the eigenfunctions of the OAM projection operator

$$\hat{L}_z = -i \frac{\partial}{\partial \phi_k} \quad (61)$$

with the eigenvalues $\lambda - \lambda'$ and $-\lambda - \lambda'$, respectively. Therefore, the vector \mathbf{F} itself is an eigenvector of the photon TAM projection operator $\hat{j}_z^{(\gamma)} = \hat{s}_z + \hat{L}_z$ with the eigenvalue $\lambda - \lambda'$.

Similarly, using the representation

$$\mathbf{n} = \boldsymbol{\chi}_0 \cos \theta_k - \frac{1}{\sqrt{2}} (\boldsymbol{\chi}_{+1} e^{-i\phi_k} - \boldsymbol{\chi}_{-1} e^{i\phi_k}) \sin \theta_k \quad (62)$$

it is not difficult to prove that the vector $\mathbf{n}(\mathbf{nF})$ and, therefore, the photon state $\mathbf{A}^{(f)}$ itself are eigenvectors of

$\hat{j}_z^{(\gamma)}$ operator with a definite value of the photon TAM projection:

$$\hat{j}_z^{(\gamma)} \mathbf{A}^{(f)} = (\lambda - \lambda') \mathbf{A}^{(f)}, \quad (63)$$

where

$$\lambda - \lambda' = \begin{cases} 0, & \text{if } \lambda' = \lambda \text{ (no electron TAM flip),} \\ 2\lambda = \pm 1, & \lambda' = -\lambda \text{ (an electron TAM flip).} \end{cases} \quad (64)$$

So, the maximum TAM value is $|j_z^{(\gamma)}| = 1$. The transverse momentum of this *Bessel beam* k_\perp equals to that of the final electron and, therefore, it can be written via the electron scattering angle θ' ,

$$k_\perp = p'_\perp = |\mathbf{p}'| \sin \theta'. \quad (65)$$

As this angle is usually negligibly small for Cherenkov radiation, $\theta' \ll 1$, it is very challenging to precisely measure the azimuthal angle ϕ' . In this sense, Cherenkov radiation with no post-selection of ϕ' can be viewed as a natural source of twisted photons, coherently emitted to

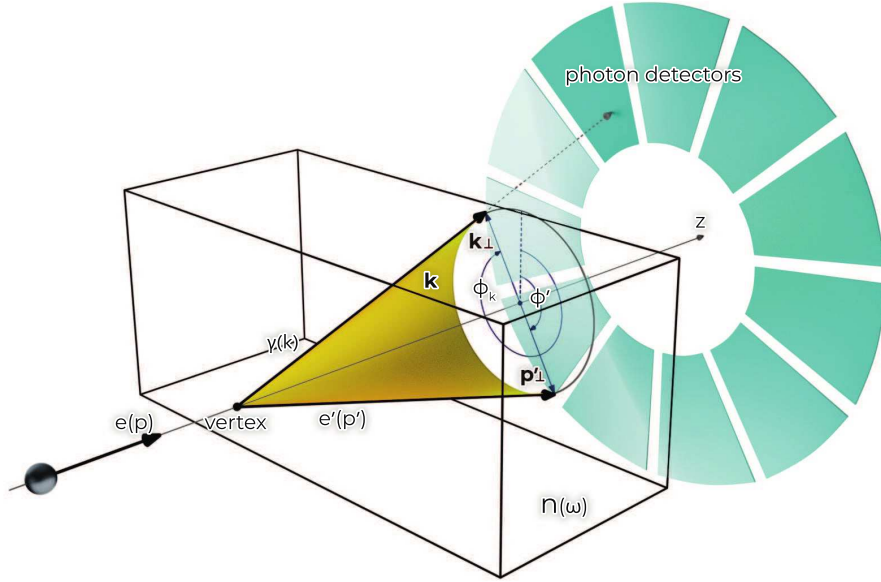


FIG. 3. An azimuthal “which-way” experiment with Cherenkov radiation: during a projective measurement of the electron momentum \mathbf{p}' we learn the photon angle ϕ_k , which is why the photon is but a plane wave. However, if the electron azimuthal angle ϕ' is measured with a large error or is not measured at all, the angle ϕ_k stays undefined, and the evolved state of the photon automatically becomes twisted with a definite TAM z -projection. In practice, the electron scattering angle is usually very small, $\theta' \ll 1$, so precise measurements of the azimuthal angle ϕ' can be very challenging. In this quasi-classical regime the photons become twisted being coherently emitted to all the azimuthal angles on the Cherenkov cone.

all the azimuthal angles on the Cherenkov cone. We emphasize that even the state with the vanishing eigenvalue of $\hat{j}_z^{(\gamma)}$ in Eq.(59) is *not* a plane wave but a cylindrical one with the *spin-orbit interaction* (SOI).

Clearly, Eq.(64) is in full agreement with the conservation law of the TAM z -projection $\hat{j}_z = \hat{j}_z' + \hat{j}_z^{(\gamma)}$. Now recall that the conservation law of the TAM takes place not only for the pure states with $\langle \hat{j}_z \rangle = \pm 1/2$, but also for the mixed states with $\langle \hat{j}_z \rangle \in [-1/2, 1/2]$, $\langle \hat{j}_z' \rangle \in [-1/2, 1/2]$. In the latter case, instead of Eq.(64) we have

$$\langle \hat{j}_z \rangle^{(\gamma)} = \langle \hat{j}_z \rangle - \langle \hat{j}_z' \rangle, \quad (66)$$

where for the mixed electron states the photon TAM lies in the interval $\langle \hat{j}_z \rangle^{(\gamma)} \in [-1, 1]$. In particular, when the initial electron is unpolarized, $\langle \hat{j}_z \rangle = 0$, and the final electron TAM is not measured, $\langle \hat{j}_z' \rangle = 0$, the photon TAM is also vanishing, although the photon is still twisted.

Finally, when the initial electron is in a pure *twisted* state [26] with the TAM z -projection

$$m = \pm 1/2, \pm 3/2, \dots, \quad (67)$$

its bispinor $u \equiv u_{p\lambda}$ with

$$\mathbf{p} = \{p_\perp \cos \phi, p_\perp \sin \phi, p_z\} \quad (68)$$

transforms as (see Eq. (26))

$$u_{p\lambda} \rightarrow u_{p_\perp p_z m \lambda} = i^{-(m-\lambda)} \int_0^{2\pi} \frac{d\phi}{2\pi} e^{i(m-\lambda)\phi} u_{p\lambda}. \quad (69)$$

The further integration over ϕ and ϕ' can be performed analytically. As a result, the photon TAM transforms as $\lambda - \lambda' \rightarrow m - \lambda'$:

$$\hat{j}_z^{(\gamma)} \mathbf{A}^{(f)} = (m - \lambda') \mathbf{A}^{(f)}. \quad (70)$$

Thus, vorticity of the incoming electron can be transferred to the photon and in this case the twisted photons with the TAM $|\hat{j}_z^{(\gamma)}| > 1$ can be emitted.

Clearly, the same post-selection protocol can also be applied for other emission processes, including synchrotron radiation, transition radiation, diffraction radiation, Smith-Purcell radiation, and so on.

V. EXAMPLE 2: NON-LINEAR COMPTON SCATTERING AND UNDULATOR RADIATION

A. Post-selection to a plane wave

In a circularly polarized laser wave with the following potential [68, 79]

$$\begin{aligned} A^\mu &= a_1^\mu \cos(kx) + a_2^\mu \sin(kx), \\ A^2 &= a_1^2 = a_2^2 = -a^2 < 0, \\ (a_1 a_2) &= (ka_1) = (ka_2) = 0, \\ kx &= \omega t - \mathbf{k} \cdot \mathbf{r} \end{aligned} \quad (71)$$

an electron is conventionally described with a Volkov state [68, 79–81]

$$\psi_{p\lambda}(\mathbf{r}, t) = N_e \left(1 + \frac{e}{2(pk)} (\gamma k)(\gamma A) \right) \times u \exp \left\{ -ipx - \frac{ie}{(pk)} \int^{kx} d\varphi \left((pA) - \frac{e}{2} A^2 \right) \right\}, \quad (72)$$

which is exact solution of the Dirac equation and where $\bar{u}u = 2m_e$, N_e is a normalization constant, and the second term in the pre-exponential factor is due to the spin,

$$(\gamma k)(\gamma A) = \frac{1}{2} \int^{kx} d\varphi F^{\mu\nu} \sigma_{\mu\nu}, \quad \sigma_{\mu\nu} = \frac{1}{2} (\gamma^\mu \gamma^\nu - \gamma^\nu \gamma^\mu), \quad F^{\mu\nu} = \partial^\mu A^\nu - \partial^\nu A^\mu. \quad (73)$$

Note that the Volkov state (72) transforms into a plane wave when the laser field is off, $A \rightarrow 0$. The case when the incoming electron is twisted and is in a Bessel-Volkov state [33] is studied hereafter. The final photon wave function is also a plane wave,

$$\mathcal{A}^\mu = N_\gamma e'^\mu e^{-i\omega' t + i\mathbf{k}' \cdot \mathbf{r}}, \quad k'_\mu e'^\mu = 0. \quad (74)$$

The corresponding matrix element is

$$S_{fi}^{(\text{pw})} = -ie \int d^4x \bar{\psi}_{p'\lambda'} \gamma_\mu \psi_{p\lambda} (\mathcal{A}^\mu)^* \quad (75)$$

where the final electron is also in the Volkov state,

$$\bar{\psi}_{p'\lambda'}(\mathbf{r}, t) = N_{e'} \bar{u}' \left(1 + \frac{e}{2(p'k)} (\gamma A)(\gamma k) \right) \times \exp \left\{ ip'x + \frac{ie}{(p'k)} \int^{kx} d\varphi \left((p'A) - \frac{e}{2} A^2 \right) \right\}. \quad (76)$$

where $\bar{u}'u' = 2m_e$.

Because this problem can be solved exactly [68, 79–81], its results can be applied for an approximate description of similar problems where an electron also moves along a helical path, the simplest example being emission in a helical undulator [82–84]. As shown, for instance, in Ref.[83], the spectral distributions of the radiated energy of both the processes are quantitatively very similar for ultrarelativistic electrons with $\varepsilon/m \gg 1$ and the small recoil $\omega'/\varepsilon \ll 1$. We emphasize that although the electron is usually post-selected to the Volkov (plane-wave) state in calculations [68, 79–81], this implies a *projective measurement* of the electron quasi-momentum q' with the vanishing uncertainties of all its components (the scheme (i) from Sec.II C).

Importantly, this may *not* necessarily happen in practice in the quasi-classical regime if we do not have complete information about the final electron state. Indeed, when the recoil is small and the electron scattering angle is vanishing, $\theta' \ll 1$, the electron stays in the laser field or inside an undulator, its energy is thereby implicitly measured, but the momentum azimuthal angle may not be known at all, simply because it is practically challenging to precisely measure it at the angles of $\theta' \sim 10^{-6} - 10^{-5}$

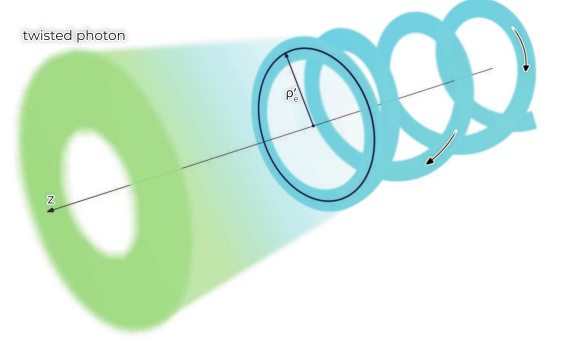


FIG. 4. A schematic picture of emission of a photon during the motion of an electron wave packet along a helical path with a mean radius $\rho'_e = ea/(p'k)$, either in a helical undulator or in a circularly polarized laser wave. The evolved state of the photon becomes twisted only if the azimuthal angle of the emitting electron momentum is measured with a large error or is not measured at all, which is typical for the quasi-classical regime with the small scattering angle, $\theta' \ll 1$. The radius of the first Bessel ring is of the order of $(p'_\perp)^{-1}$, which is usually larger than ρ'_e according to Eq.(106).

rad. In this regime, the electron quasi-momentum is measured within the scheme (iii) from Sec.II C, and the photon itself is automatically projected to the twisted state (see Fig.4). We will return to this generalized-measurement scheme in the next sub-section.

Following the standard procedure [68, 79–81], we expand the matrix element into series over the harmonic number $s \geq 1$, regroup the terms in the pre-exponential factor with the same indices of the Bessel functions J_s and $J_{s\pm 1}$, and represent the result as follows:

$$S_{fi}^{(\text{pw})} = \sum_{s=1}^{\infty} S_{fi}^{(s)} = -ieN \sum_{s=1}^{\infty} (2\pi)^4 \delta^{(4)}(q + sk - q' - k') \times \sum_{\sigma=0,\pm 1} (e'_\mu)^* \bar{u}' \Gamma_\sigma^\mu u J_{s+\sigma}(\Sigma) e^{i(s+\sigma)\xi}. \quad (77)$$

Here, $N = N_e N_{e'} N_\gamma$ is a normalization constant, the electron quasi-momenta are

$$q^\mu = p^\mu + e^2 k^\mu \frac{a^2}{2(pk)}, \quad (q')^\mu = (p')^\mu + e^2 k^\mu \frac{a^2}{2(p'k)} \quad (78)$$

and we have also denoted

$$\Sigma = e \sqrt{\left(\frac{pa_1}{(pk)} - \frac{p'a_1}{(p'k)} \right)^2 + \left(\frac{pa_2}{(pk)} - \frac{p'a_2}{(p'k)} \right)^2}, \quad \xi = \arctan \frac{(pa_2)/(pk) - (p'a_2)/(p'k)}{(pa_1)/(pk) - (p'a_1)/(p'k)}. \quad (79)$$

The “dressed” vertex Γ_σ^μ is

$$\begin{aligned}
\Gamma_\sigma^\mu &= \{\Gamma_0^\mu, \Gamma_{+1}^\mu, \Gamma_{-1}^\mu\} = \\
&= \left\{ \gamma^\mu - k^\mu \frac{e^2 A^2}{2(pk)(p'k)} (\gamma k), \frac{1}{2} (\gamma a_-) \left(\frac{e}{2} (\gamma k) \gamma^\mu \left(\frac{1}{(p'k)} - \frac{1}{(pk)} \right) + k^\mu \frac{e}{(pk)} \right) - a_-^\mu \frac{e}{2(pk)} (\gamma k), \right. \\
&\quad \left. \frac{1}{2} (\gamma a_+) \left(\frac{e}{2} (\gamma k) \gamma^\mu \left(\frac{1}{(p'k)} - \frac{1}{(pk)} \right) + k^\mu \frac{e}{(pk)} \right) - a_+^\mu \frac{e}{2(pk)} (\gamma k) \right\}, \\
a_\pm^\mu &= a_1^\mu \pm i a_2^\mu, (ka_\pm) = 0.
\end{aligned} \tag{80}$$

We emphasize that these expressions are still the standard ones for the non-linear Compton scattering [68, 79–

81], just written differently.

In what follows, we only study the head-on collision, for which

$$\begin{aligned}
p &= \{\varepsilon, 0, 0, |\mathbf{p}|\}, \quad k = \{\omega, 0, 0, -\omega\}, \quad k' = \{\omega', k'_\perp \cos \phi_{k'}, k'_\perp \sin \phi_{k'}, k'_z\}, \quad k'_\perp = \omega' \sin \theta_{k'}, \\
p' &= \{\varepsilon', p'_\perp \cos \phi', p'_\perp \sin \phi', p'_z\}, \quad p'_\perp = |\mathbf{p}'| \sin \theta', \\
a_1^\mu &= a\{0, 1, 0, 0\}, \quad a_2^\mu = a\{0, 0, 1, 0\}, \\
a_\pm^\mu &= a\{0, \mathbf{e}_\pm\}, \quad \mathbf{e}_\pm = \hat{\mathbf{x}} \pm i \hat{\mathbf{y}}, \quad \hat{\mathbf{x}} = \{1, 0, 0\}, \quad \hat{\mathbf{y}} = \{0, 1, 0\}, \\
\delta^{(4)}(q + sk - q' - k') &= \delta(q^0 + s\omega - (q')^0 - \omega') \delta(q_z + sk_z - q'_z - k'_z) \delta^{(2)}(\mathbf{p}'_\perp + \mathbf{k}'_\perp),
\end{aligned} \tag{81}$$

and the transverse delta-function can again be represented in cylindrical coordinates, according to Eq.(39). In this case,

$$(pa_1) = (pa_2) = 0, \tag{82}$$

the vertex Γ_σ^μ does not depend on the azimuthal angles of the final particles, and so

$$\tan \xi = \frac{p'_y}{p'_x} = \tan \phi' \Rightarrow \xi = \phi' + \pi g, \quad g = 0, 1, 2, \dots \tag{83}$$

For $g = 0$, we have

$$\xi = \phi' = \phi_{k'} \pm \pi \tag{84}$$

due to the transverse delta-function. The argument of the Bessel functions becomes

$$\Sigma = \frac{ea}{(p'k)} p'_\perp = \frac{ea}{(p'k)} k'_\perp \equiv \rho'_e k'_\perp, \tag{85}$$

where

$$\rho'_e = \frac{ea}{(p'k)} = \eta \frac{m_e}{(p'k)} \tag{86}$$

is a classical radius of the final electron path (see the problem No.2 to Sec.47 in Ref.[85] and Fig.4) and

$$\eta = \frac{e\sqrt{-A^2}}{m_e} = \frac{ea}{m_e} \tag{87}$$

is a classical field strength parameter [68, 79–81]. Thus, the radius of the classical helical trajectory inside the laser wave *naturally arises* in the quantum theory. For an optical photon and a relativistic electron, we have roughly

$$\begin{aligned}
\rho'_e &\sim \eta \lambda_c \frac{m_e}{\varepsilon'} \frac{m_e}{\omega} \sim \frac{\eta}{\gamma'} \times 0.1 [\mu\text{m}], \\
\gamma' &= \varepsilon'/m_e, \quad \lambda_c = 1/m_e,
\end{aligned} \tag{88}$$

which reaches the atomic scale,

$$\rho'_e \sim 0.1 \text{ nm} - 1 \text{ nm}, \tag{89}$$

for $\gamma' \sim 10 - 100, \eta \sim 0.1 - 1$.

Thus, the evolved state of the emitted photon (10) looks as follows:

$$\begin{aligned}
\mathbf{A}^{(f)}(\mathbf{k}', \omega') &= \sum_{s=1}^{\infty} \mathbf{A}^{(f,s)}(\mathbf{k}', \omega'), \\
\mathbf{k}' \cdot \mathbf{A}^{(f,s)} &= 0, \quad \mathbf{n}' = \mathbf{k}'/\omega', \\
\mathbf{A}^{(f,s)}(\mathbf{k}', \omega') &= -ieN(2\pi)^4 \delta^{(4)}(q + sk - q' - k') \\
&\times \sum_{\lambda_\gamma = \pm 1} \sum_{\sigma=0, \pm 1} \mathbf{e}' e'^* \bar{u}' \Gamma_\sigma^\mu u J_{s+\sigma}(\rho'_e k'_\perp) e^{i(s+\sigma)\phi'},
\end{aligned} \tag{90}$$

where the sum over σ has appeared because of the spin terms (73). Summation over the photon helicities λ_γ is done as in Eq.(58). Then, choosing the final electron bispinor as an eigenstate of \hat{j}'_z operator with the eigenvalue $\lambda' = \pm 1/2$, as in Sec.III A, the evolved state becomes

$$\begin{aligned}
&\mathbf{A}^{(f,s)}(\mathbf{k}', \omega') = -ieN(2\pi)^4 \delta^{(4)}(q + sk - q' - k') \\
&\times \mathbf{n}' \times \left[\mathbf{n}' \times \sum_{\sigma' = \pm 1/2} \sum_{\sigma=0, \pm 1} d_{\sigma'\lambda'}^{(1/2)}(\theta') \bar{u}_{\varepsilon'\lambda'}^{(\sigma')} \Gamma_\sigma u J_{s+\sigma}(\rho'_e k'_\perp) e^{i(s+\sigma+\sigma'-\lambda')\phi'} \right].
\end{aligned} \tag{91}$$

where we have expanded the final electron bispinor according to Eq.(46). Clearly, this wave function is just a plane wave with the vanishing z -projection of the OAM because the photon has the definite 4-momentum k' and the azimuthal angle $\phi_{k'}$.

B. Post-selection with a generalized measurement

1. General analysis

In the standard projective-measurement scheme, we detect photons emitted in a laser wave or in a helical undulator with a detector placed at an angle $\phi_{k'}$, which automatically projects the electron to the plane-wave (Volkov) state $|\mathbf{q}', \lambda'\rangle$ with $\phi' = \phi_{k'} \pm \pi$. However, if

we do not measure the electron angle ϕ' alone, as often takes place in the quasiclassical regime with the small scattering angle, $\theta' \ll 1$, then the photon itself evolves to the twisted state, irrespectively of how we detect it. The electron detected state in the generalized-measurement scheme with the maximized error is

$$|e'_{\text{det}}\rangle^{(g)} = \int_0^{2\pi} \frac{d\phi'}{2\pi} |\mathbf{q}', \lambda'\rangle, \quad (92)$$

and the information about the electron quasi-momentum \mathbf{q}' is incomplete. Importantly, in the head-on geometry (81) we have $\mathbf{p}'_{\perp} = \mathbf{q}'_{\perp}$, and so the azimuthal angles of both the vectors *coincide*.

We can obtain the evolved photon wave function by integrating Eq.(91)

$$\begin{aligned} \mathbf{A}_{(g)}^{(f,s)}(\mathbf{k}', \omega') &= \int_0^{2\pi} \frac{d\phi'}{2\pi} \mathbf{A}^{(f,s)}(\mathbf{k}', \omega') = \\ &= -ieN(2\pi)^3 \delta(q^0 + s\omega - (q')^0 - \omega') \delta(q_z + sk_z - q'_z - k'_z) \frac{1}{k'_{\perp}} \delta(p'_{\perp} - k'_{\perp}) \\ &\times \mathbf{n}' \times \left[\mathbf{n}' \times \sum_{\sigma'=\pm 1/2} \sum_{\sigma=0,\pm 1} d_{\sigma'\lambda'}^{(1/2)}(\theta') \bar{u}_{\epsilon'\lambda'}^{(\sigma')} \mathbf{\Gamma}_{\sigma} u J_{s+\sigma}(\rho'_{\epsilon} k'_{\perp}) e^{i(s+\sigma+\sigma'-\lambda')(\phi_{k'} \pm \pi)} \right]. \end{aligned} \quad (93)$$

Even without the calculation of $\bar{u}_{\epsilon'\lambda'}^{(\sigma')} \mathbf{\Gamma}_{\sigma} u$, it is now clear that the photon represents a cylindrical wave with the SOI.

Next, we use the representation

$$\bar{u}_{\epsilon'\lambda'}^{(\sigma')} \mathbf{\Gamma}_{\sigma} u = \mathbf{G}^{(\uparrow\uparrow)} \delta_{\lambda,\sigma'} + \mathbf{G}^{(\uparrow\downarrow)} \delta_{\lambda,-\sigma'}, \quad (94)$$

where the vectors $\mathbf{G}^{(\uparrow\uparrow)} \equiv \mathbf{G}_{\sigma\lambda'\lambda}^{(\uparrow\uparrow)}$, $\mathbf{G}^{(\uparrow\downarrow)} \equiv \mathbf{G}_{\sigma\lambda'\lambda}^{(\uparrow\downarrow)}$ are found as

$$\begin{aligned} \mathbf{G}_{0\lambda'\lambda}^{(\uparrow\uparrow)} &= \chi_0 \left(f_{\lambda'\lambda}^{(2)} - \frac{\eta^2 m_e^2 \omega^2}{2(pk)(p'k)} (f_{\lambda'\lambda}^{(1)} + f_{\lambda'\lambda}^{(2)}) \right), \\ \mathbf{G}_{0\lambda'\lambda}^{(\uparrow\downarrow)} &= -f_{\lambda'\lambda}^{(2)} \sqrt{2} \chi_{2\lambda}, \\ \mathbf{G}_{\pm 1\lambda'\lambda}^{(\uparrow\uparrow)} &= \mp \sqrt{2} \chi_{\mp 1} \frac{\eta m_e \omega}{2} (f_{\lambda'\lambda}^{(1)} + f_{\lambda'\lambda}^{(2)}) \left(\delta_{\lambda,\mp 1/2} \left(\frac{1}{(p'k)} - \frac{1}{(pk)} \right) + \frac{1}{(pk)} \right), \\ \mathbf{G}_{\pm 1\lambda'\lambda}^{(\uparrow\downarrow)} &= \mp \chi_0 \frac{\eta m_e \omega}{2} \delta_{\lambda,\pm 1/2} \left(\left(\frac{1}{(p'k)} - \frac{1}{(pk)} \right) (f_{\lambda'\lambda}^{(1)} - f_{\lambda'\lambda}^{(2)}) - \frac{2f_{\lambda'\lambda}^{(2)}}{(pk)} \right), \\ f_{\lambda'\lambda}^{(1)} &= \sqrt{\varepsilon + m_e} \sqrt{\varepsilon' + m_e} + 2\lambda 2\lambda' \sqrt{\varepsilon - m_e} \sqrt{\varepsilon' - m_e}, \\ f_{\lambda'\lambda}^{(2)} &= \sqrt{\varepsilon - m_e} \sqrt{\varepsilon' + m_e} + 2\lambda 2\lambda' \sqrt{\varepsilon + m_e} \sqrt{\varepsilon' - m_e}. \end{aligned} \quad (95)$$

Note that they do not explicitly depend on the 4-momentum k' of the final photon. The vectors $\chi_0, \chi_{\pm 1}$

are given in Eq.(50).

The final expression for the wave function is

$$\mathbf{A}_{(g)}^{(f,s)}(\mathbf{k}', \omega') = -ie(-1)^{s+\lambda-\lambda'} N(2\pi)^3 \delta(q^0 + s\omega - (q')^0 - \omega') \delta(q_z + sk_z - q'_z - k'_z) \frac{1}{k'_{\perp}} \delta(p'_{\perp} - k'_{\perp})$$

$$\times \mathbf{n}' \times \left[\mathbf{n}' \times \sum_{\sigma=0,\pm 1} J_{s+\sigma}(\rho'_e k'_\perp) e^{i(s+\sigma-\lambda')\phi_{k'}} \left(d_{\lambda\lambda'}^{(1/2)}(\theta') \mathbf{G}_{\sigma\lambda'\lambda}^{(\uparrow\uparrow)} e^{i\lambda\phi_{k'}} + d_{-\lambda\lambda'}^{(1/2)}(\theta') \mathbf{G}_{\sigma\lambda'\lambda}^{(\uparrow\downarrow)} e^{-i\lambda\phi_{k'}} \right) \right], \quad (96)$$

which is obviously a *Bessel beam* with the SOI, revealed by the sum over σ , and the following TAM projection:

$$\hat{j}_z^{(\gamma)} \mathbf{A}_{(g)}^{(f,s)} = (s + \lambda - \lambda') \mathbf{A}_{(g)}^{(f,s)}, \quad (97)$$

whereas the TAM uncertainty is vanishing. Here, in contrast to Eq.(64) for Cherenkov radiation above, the harmonic number $s = 1, 2, 3, \dots$ appears in the r.h.s. For the unpolarized electrons with $\langle \hat{j}_z \rangle = \langle \hat{j}'_z \rangle = 0$, the photon TAM is simply s .

Analogously to Cherenkov radiation, the transverse momentum of this Bessel photon is defined by the electron scattering angle θ' as

$$k'_\perp = |\mathbf{p}'| \sin \theta'. \quad (98)$$

Importantly, the twisted photons can also be generated in the genuinely quantum non-linear regime with $\eta \sim \theta' \sim 1$, but only when the electron azimuthal angle is measured with a large error.

If needed, one can also obtain the Bessel beam in the coordinate representation according to Eq.(12). To this end, it is convenient to divide the vector potential (96) into the following parts:

$$\begin{aligned} \mathbf{A}_{(g)}^{(f,s)} &\equiv \mathbf{A}_{\mathbf{G}}^{(f,s)} + \mathbf{A}_{\mathbf{n}'}^{(f,s)}, \\ \mathbf{A}_{\mathbf{G}}^{(f,s)} &\propto \mathbf{G}, \quad \mathbf{A}_{\mathbf{n}'}^{(f,s)} \propto \mathbf{n}'(\mathbf{n}' \cdot \mathbf{G}), \end{aligned} \quad (99)$$

where \mathbf{G} is either $\mathbf{G}_{\sigma\lambda'\lambda}^{(\uparrow\uparrow)}$ or $\mathbf{G}_{\sigma\lambda'\lambda}^{(\uparrow\downarrow)}$. For the former part, we obtain

$$\begin{aligned} \mathbf{A}_{\mathbf{G}}^{(f,s)}(\mathbf{r}, \omega') &= ie(-1)^{s+\lambda-\lambda'} N 2\pi \delta(q^0 + s\omega - (q')^0 - \omega') e^{iz(q_z + sk_z - q'_z)} \\ &\times \sum_{\sigma=0,\pm 1} i^{s+\sigma-\lambda'} J_{s+\sigma}(\rho'_e p'_\perp) e^{i(s+\sigma-\lambda')\phi_r} \left(i^\lambda d_{\lambda\lambda'}^{(1/2)}(\theta') \mathbf{G}_{\sigma\lambda'\lambda}^{(\uparrow\uparrow)} e^{i\lambda\phi_r} J_{s+\sigma-\lambda'+\lambda}(\rho p'_\perp) + \right. \\ &\quad \left. + i^{-\lambda} d_{-\lambda\lambda'}^{(1/2)}(\theta') \mathbf{G}_{\sigma\lambda'\lambda}^{(\uparrow\downarrow)} e^{-i\lambda\phi_r} J_{s+\sigma-\lambda'-\lambda}(\rho p'_\perp) \right), \end{aligned} \quad (100)$$

where ϕ_r is the azimuthal angle of the vector

$$\mathbf{r} = \{\rho \cos \phi_r, \rho \sin \phi_r, z\}, \quad (101)$$

and the following identity has been used

$$\int_0^{2\pi} \frac{d\phi}{2\pi} e^{ix \cos \phi + i\ell \phi} = i^\ell J_\ell(x). \quad (102)$$

Clearly, the part $\mathbf{A}_{\mathbf{n}'}^{(f,s)}(\mathbf{r}, \omega')$ is much more cumbersome, whereas the momentum representation above is more compact.

The spatial distributions of the energy of this Bessel beam

$$|\dot{\mathbf{E}}_{(g)}^{(f,s)}|^2 = \frac{1}{T} \int d\omega' |\mathbf{E}_{(g)}^{(f,s)}(\mathbf{r}, \omega')|^2 \quad (103)$$

represent a typical doughnut, as shown in Fig.5. Here T is a very large ‘‘observation time’’ obtained when squaring the delta-function in Eq.(100) (see, e.g., [68]). Importantly, whereas the radius of the emitting electron classical path (86) does not change much during the emission of soft photons, $\rho'_e \approx \rho_e$, the radius of the first Bessel ring is of the order of $1/p'_\perp \approx 1/\varepsilon'\theta'$, which *does not necessarily coincide* with ρ_e . Indeed, the electron scattering angle is usually small and limited from above [86],

$$\theta' \leq \frac{2s}{\sqrt{1+\eta^2}} \frac{\omega}{m_e}, \quad (104)$$

so the photon transverse momentum is

$$k'_\perp \leq \varepsilon' \frac{2s}{\sqrt{1+\eta^2}} \frac{\omega}{m_e}, \quad (105)$$

and it can reach the keV scale for GeV electrons and optical laser photons. That is why in the relativistic case we have

$$\frac{(p'_\perp)^{-1}}{\rho'_e} \approx \frac{2}{\eta} \frac{\omega}{m_e} \frac{1}{\theta'} \geq \frac{\sqrt{1+\eta^2}}{s\eta}. \quad (106)$$

Very roughly, one can think of $(k'_\perp)^{-1} = (p'_\perp)^{-1}$ as of *the transverse coherence length* of the twisted photon, although this quantity cannot be quantitatively defined for an unnormalized Bessel beam. Thus, in the linear regime with $\eta \ll 1$ the radius of the first Bessel ring is much larger than the radius of the electron classical path, while in the non-linear regime with $\eta \gtrsim 1$ this ratio is of the order of unity, as shown in Fig.4. The opposite case with $\eta \gg 1$ corresponds to a constant crossed field instead of the plane wave [68, 79], and the above ratio gets larger than $1/s$.

2. Quasi-classical regime

Let us study in more detail the emission of soft twisted photons, $\omega' \ll \varepsilon$, by a relativistic electron, $\varepsilon \gg m_e$,

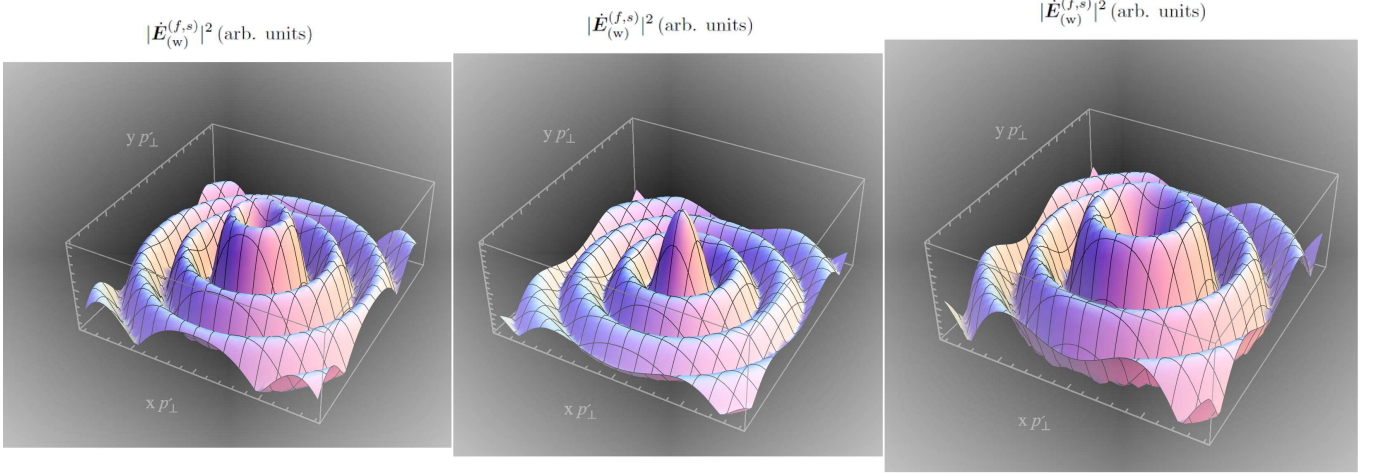


FIG. 5. The energy spatial distributions (103) of the Bessel photon emitted in the non-linear Compton scattering within the generalized-measurement scheme (iii) with the electron azimuthal angle being measured with a very large error or not measured at all. Left panel: $\omega = 5 \text{ eV}$, $\varepsilon/m_e = 10$, $\varepsilon' = 0.9999 \varepsilon$, $\theta' \approx 10^{-5} \text{ rad}$, $\eta = 0.5$, $s = 1$, $\lambda = -1/2$, $\lambda' = 1/2$ (a spin flip), $j_z^{(\gamma)} = s + \lambda - \lambda' = 0$. Central panel: the same, but $\lambda = 1/2$, $\lambda' = 1/2$ (no spin flip), $j_z^{(\gamma)} = s + \lambda - \lambda' = 1$. Right panel: $\omega = 0.5 \text{ eV}$, $\varepsilon/m_e = 100$, $\varepsilon' = 0.9999 \varepsilon$, $\theta' \approx 10^{-6} \text{ rad}$, $\eta = 0.5$, $s = 3$, $\lambda = 1/2$, $\lambda' = 1/2$ (no spin flip), $j_z^{(\gamma)} = s + \lambda - \lambda' = 3$. Everywhere $(p'_\perp)^{-1} \approx 4 \text{ nm} \approx 4\rho'_e$, so the Bessel rings are wider than the radius of the electron classical path ρ'_e (86) according to Eq.(106).

which stays relativistic after the emission, $\varepsilon' \gg m_e$. The radiated energy is concentrated at the small angles,

$$\theta_{k'} \ll 1. \quad (107)$$

We call this *the quasi-classical regime*. Due to the delta-function $\delta(p'_\perp - k'_\perp)$ in Eq.(93),

$$\sin \theta' / \sin \theta_{k'} = \frac{\omega'}{|\mathbf{p}'|} \approx \frac{\omega'}{\varepsilon'} \ll 1, \quad (108)$$

which is why the electron scattering angle θ' is yet smaller than the photon emission angle,

$$\theta' \ll \theta_{k'} \ll 1. \quad (109)$$

In this case

$$d_{\sigma\lambda}^{(1/2)}(\theta') = \delta_{\sigma\lambda} + O(\theta'), \quad (110)$$

and only the term with $\sigma = -1$ survives in the sum in Eq.(96) in the leading approximation,

$$\begin{aligned} \mathbf{A}_{(g)}^{(f,s)}(\mathbf{k}', \omega') &\propto \sum_{\sigma=0,\pm 1} \equiv \sum_{\sigma=0,\pm 1} J_{s+\sigma}(\rho'_e k'_\perp) e^{i(s+\sigma-\lambda')\phi_{k'}} \left(d_{\lambda\lambda'}^{(1/2)}(\theta') \mathbf{G}_{\sigma\lambda'\lambda}^{(\uparrow\uparrow)} e^{i\lambda\phi_{k'}} + d_{-\lambda\lambda'}^{(1/2)}(\theta') \mathbf{G}_{\sigma\lambda'\lambda}^{(\uparrow\downarrow)} e^{-i\lambda\phi_{k'}} \right) \approx \\ &\approx \frac{(\rho'_e \omega' \theta_{k'})^{s-1}}{2^{s-1}(s-1)!} e^{i(s-1)\phi_{k'}} \left(\delta_{\lambda\lambda'} \mathbf{G}_{-1\lambda'\lambda}^{(\uparrow\uparrow)} + \delta_{-\lambda\lambda'} \mathbf{G}_{-1\lambda'\lambda}^{(\uparrow\downarrow)} \right) \end{aligned} \quad (111)$$

where we have only taken the first term in expansion of the Bessel function in series,

$$J_{s-1}(\rho'_e k'_\perp) \approx \frac{(\rho'_e \omega' \theta_{k'})^{s-1}}{2^{s-1}(s-1)!}. \quad (112)$$

In other words, the SOI vanishes in this approximation.

Indeed, the fact that only the term with $\sigma = -1$ survives for relativistic energies is the reason why we have

a minimum at $\rho = 0$ for $j_z^{(\gamma)} = 0$ in the left panel of Fig.5, whereas there is a maximum in the central panel at $\rho = 0$ for $j_z^{(\gamma)} = 1$. The Bessel function in Eq.(100) that defines the shape of these distributions is $J_{j_z+\sigma}(\rho p'_\perp) \rightarrow J_{j_z-1}(\rho p'_\perp)$, which yields J_1 in the former case and J_0 in the latter.

As follows from the r.h.s. of Eq.(111), the term with

$\mathbf{G}^{(\uparrow\uparrow)}$ corresponds to the emission *without an electron spin flip*, whereas the term with $\mathbf{G}^{(\uparrow\downarrow)}$ implies that the *electron spin flips* when the photon is emitted. Now let us recall that the vectors $\mathbf{G}^{(\uparrow\uparrow)}$, $\mathbf{G}^{(\uparrow\downarrow)}$ only depend on the electron energies but not on the emission angles $\theta_{k'}$, $\phi_{k'}$. As can be easily seen from Eq.(95), the following estimates hold in the relativistic case,

$$\begin{aligned} f_{\lambda\lambda}^{(1)} + f_{\lambda\lambda}^{(2)} &\approx 4\sqrt{\varepsilon\varepsilon'}, \\ f_{-\lambda\lambda}^{(1)} - f_{-\lambda\lambda}^{(2)} &\approx 2\sqrt{\varepsilon\varepsilon'} \frac{m}{\varepsilon}, \end{aligned}$$

$$f_{-\lambda\lambda}^{(2)} \approx \sqrt{\varepsilon\varepsilon'} \left(\frac{m}{\varepsilon'} - \frac{m}{\varepsilon} \right). \quad (113)$$

As a result

$$|\mathbf{G}_{-1-\lambda\lambda}^{(\uparrow\downarrow)}|/|\mathbf{G}_{-1\lambda\lambda}^{(\uparrow\uparrow)}| = \mathcal{O}(m/\varepsilon), \quad (114)$$

because $\varepsilon' \lesssim \varepsilon$. In other words, the amplitude with an electron spin flip $\delta_{-\lambda\lambda'} \mathbf{G}_{-1-\lambda\lambda}^{(\uparrow\downarrow)}$ is roughly $\varepsilon/m \gg 1$ times smaller than the amplitude $\delta_{\lambda\lambda'} \mathbf{G}_{-1\lambda\lambda}^{(\uparrow\uparrow)}$ without the spin flip, which looks natural for the quasi-classical regime. As a result, only $\mathbf{G}_{-1\lambda\lambda}^{(\uparrow\uparrow)}$ survives and we finally get

$$\begin{aligned} \mathbf{A}_{(g)}^{(f,s)}(\mathbf{k}', \omega') &\propto \sum_{\sigma=0,\pm 1} \approx \frac{(\rho'_e \omega' \theta_{k'})^{s-1}}{2^{s-1}(s-1)!} e^{i(s-1)\phi_{k'}} \delta_{\lambda\lambda'} \mathbf{G}_{-1\lambda\lambda}^{(\uparrow\uparrow)}, \\ \mathbf{G}_{-1\lambda\lambda}^{(\uparrow\uparrow)} &\approx 2\sqrt{2} \eta m_e \omega \sqrt{\varepsilon\varepsilon'} \chi_{+1} \left(\delta_{\lambda,1/2} \left(\frac{1}{(p'k')} - \frac{1}{(pk)} \right) + \frac{1}{(pk)} \right). \end{aligned} \quad (115)$$

When the electron recoil is completely neglected (the classical limit or the Thomson scattering), we have

$$\varepsilon' \rightarrow \varepsilon, \omega' \rightarrow s\omega, \quad (116)$$

and so

$$\begin{aligned} \mathbf{G}_{-1\lambda\lambda}^{(\uparrow\uparrow)} &\approx 2\sqrt{2} \rho_e \omega \varepsilon \chi_{+1}, \\ &\sum_{\sigma=0,\pm 1} \approx \\ &\approx 2\sqrt{2} \varepsilon (\rho_e \omega)^s \frac{(s \theta_{k'})^{s-1}}{2^{s-1}(s-1)!} e^{i(s-1)\phi_{k'}} \delta_{\lambda\lambda'} \chi_{+1} \end{aligned} \quad (117)$$

where $\rho_e = ea/(pk) = \rho'_e = ea/(p'k)$ is the classical radius of the electron helical path in the plane wave from Eq.(86); see Ref.[85]. In Fig.6 we present comparison of the general angular dependence of $|\mathbf{A}_{(g)}^{(f,s)}(\mathbf{k}', \omega')|^2$, mostly defined by the Bessel function with $\sigma = -1$, versus the paraxial behaviour (117). The difference is only at the angles $\theta_{k'} \gg m_e/\varepsilon$.

With these approximations, we have

$$\hat{j}_z \mathbf{A}_{(g)}^{(f,s)} = s \mathbf{A}_{(g)}^{(f,s)}. \quad (118)$$

The angular distribution and the phase in Eq.(117) *exactly coincide with those of the far-field undulator radiation* (see the appendix B), whereas the TAM (118) is in accord with the classical calculations for the undulator radiation and for the non-linear Thomson scattering [10–12, 18–20] illustrating the correspondence principle.

Thus, not only the emitted energy distributions $|\mathbf{E}_{(g)}^{(f,s)}|^2$ are nearly the same for Compton scattering and for emission in a helical undulator in the quasi-classical regime [83], but *the phases of the fields do also coincide* in this approximation. Importantly, however, the phase $e^{i(s-1)\phi_{k'}}$ itself does not guarantee that the field carries angular momentum because the overall factor with the

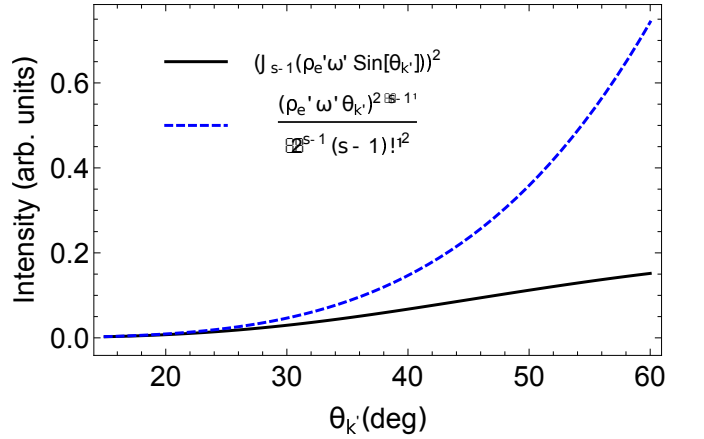


FIG. 6. The angular distributions of $|\mathbf{A}_{(g)}^{(f,s)}(\mathbf{k}', \omega')|^2$ in the quasi-classical regime with no SOI, defined by $(J_{s-1}(\rho'_e \omega' \sin \theta_{k'}))^2$ according to Eq.(96) or by its first expansion term (112). The latter dependence also takes place for undulator radiation at $\varepsilon \gg m_e$. Parameters: $\omega = 5 \text{ eV}$, $\varepsilon/m_e = 100$ ($m_e/\varepsilon \approx 0.57 \text{ deg}$), $\varepsilon' = 0.9999 \varepsilon$, $\theta' \approx 10^{-5} \text{ rad}$, $\eta = 0.5$, $s = 3$.

delta-function also plays a role. For instance, if the latter factor contains $\delta(\phi'_k - (\phi' \pm \pi))$ within the conventional plane-wave approach, the TAM z -projection is vanishing, regardless of the phase. It is only the generalized-measurement scheme with a finite error that provides vorticity of the final photons because the latter turn out to be cylindrical rather than plane waves.

3. Bessel-Volkov electron

Let us now turn to the case when the incoming electron is twisted with the TAM $m = \pm 1/2, 3/2, \dots$ and it is in the Bessel-Volkov state [33]. Clearly, this time we obtain

$$\hat{j}_z^{(\gamma)} \mathbf{A}_{(g)}^{(f,s)} = (s + m - \lambda') \mathbf{A}_{(g)}^{(f,s)}, \quad (119)$$

whereas the most general formula for the mixed states is

$$\langle \hat{j}_z \rangle^{(\gamma)} = s + \langle \hat{j}_z \rangle - \langle \hat{j}'_z \rangle. \quad (120)$$

Thus, highly twisted photons with $\langle \hat{j}_z^{(\gamma)} \rangle \gg 1$ can be obtained via the non-linear Compton effect

- Either by using the plane-wave (Volkov) incoming electrons and a powerful laser with $\eta \gtrsim 1$, so that the higher harmonics with $s > 1$ are generated,
- Or, alternatively, by taking a *moderately powerful* laser, for which only the linear scattering with $s = 1$ takes place, but with an incoming vortex (Bessel-Volkov) electron with $|m| \gg 1$.

As the highly twisted electrons with $m \sim 100 - 1000$ have already been obtained [26], the latter scheme seems to be technically easier. Besides, if the vortex electron is ultra-relativistic, the energy of the scattered highly twisted photons can easily reach MeV range [6]. The means for accelerating the vortex electrons to ultrarelativistic energies have been recently discussed in Ref.[53].

We emphasize that in the quantum regime the twisted photons are *not naturally generated* in a circularly-polarized laser wave or in a helical undulator, as it seems from the classical theory [10–12, 18–20]. In quantum approach, the photon turns out to be twisted only if the measurement error of the azimuthal angle of the final electron momentum is large. When the recoil angle θ' is small, the angle ϕ' simply loses its sense, which is why this generalized-measurement scheme reproduces results of the classical theory.

VI. EXAMPLE 3: HEAVIER PARTICLES

A. Leptons

An advantage of the generalized-measurement technique is that it can in principle be applied to particles of any mass, spin, and energy, including composite particles. We start with the QED scattering with a lepton heavier than electron,

$$e^\pm \mu^\pm \rightarrow e^\pm \mu^\pm \quad \text{or} \quad e^\pm \tau^\pm \rightarrow e^\pm \tau^\pm. \quad (121)$$

For definiteness we take the process

$$e^-(p_1) + \mu^-(p_2) \rightarrow e^-(p_3) + \mu^-(p_4) \quad (122)$$

as an example, where the electron and the muon collide head-on and have the momenta

$$p_1 = \{\varepsilon_1, 0, 0, |\mathbf{p}_1|\}, \quad \varepsilon_1 = \sqrt{m_e^2 + |\mathbf{p}_1|^2}, \\ \text{and} \quad p_2 = \{\varepsilon_2, 0, 0, -|\mathbf{p}_2|\}, \quad \varepsilon_2 = \sqrt{m_\mu^2 + |\mathbf{p}_2|^2}, \quad (123)$$

as well as the helicities λ_1, λ_2 , respectively. When the final electron is detected in the generalized-measurement scheme, the evolved wave function of the muon, according to Eq.(40), becomes

$$\psi_\mu^{(f)} = \sum_{\lambda_4 = \pm 1/2} \int_0^{2\pi} \frac{d\phi_3}{2\pi} u_4 S_{fi}^{(\text{pw})}, \quad (124)$$

where $u_4 \equiv u_{p_4 \lambda_4}$ and the matrix element reads

$$S_{fi}^{(\text{pw})} = i(2\pi)^4 N \delta^{(4)}(p_1 + p_2 - p_3 - p_4) \\ \times \frac{4\pi e^2}{q^2} (\bar{u}_3 \gamma^\alpha u_1) (\bar{u}_4 \gamma_\alpha u_2), \quad q = p_1 - p_3, \quad (125)$$

where the photon propagator is taken in the Feynman gauge. In contrast to the previous section, the 4-vector q is a momentum transfer.

The muon current can be presented as

$$\bar{u}_4 \gamma_\alpha u_2 = J_\alpha^{(\mu)} e^{-i(\lambda_2 + \lambda_4)\phi_4}, \quad (126)$$

where $J_\alpha^{(\mu)}$ is given in Eq.(53) with $m_e \rightarrow m_\mu$. After the integration, the electron current becomes

$$\int_0^{2\pi} d\phi_3 \delta(\phi_3 - (\phi_4 \pm \pi)) \bar{u}_3 \gamma_\alpha u_1 = \\ = J_\alpha^{(e)}(\phi_3 = \phi_4 \pm \pi) e^{i(\lambda_1 - \lambda_3)(\phi_4 \pm \pi)}. \quad (127)$$

Taking into account that

$$\boldsymbol{\chi}_{-2\lambda_2} \cdot \boldsymbol{\chi}_{2\lambda_1} = -\delta_{\lambda_2 \lambda_1}, \quad (128)$$

it is easy to check that the scalar product

$$\mathcal{J} \equiv J_\alpha^{(e)}(\phi_3 = \phi_4 \pm \pi) (J^{(\mu)})^\alpha \quad (129)$$

does not depend on ϕ_4 . Therefore,

$$\psi_\mu^{(f)} \propto \sum_{\lambda_4 = \pm 1/2} \tilde{u}_4 \mathcal{J} e^{i(\lambda_1 - \lambda_2 - \lambda_3)\phi_4}, \quad (130)$$

where $\tilde{u}_4 = u_4 e^{-i\lambda_4 \phi_4}$ has a vanishing TAM, see Eq.(45). As a result,

$$\hat{j}_{4,z} \psi_\mu^{(f)} = (\lambda_1 - \lambda_2 - \lambda_3) \psi_\mu^{(f)}, \quad (131)$$

i.e. the muon becomes twisted.

Similarly, for the twisted incoming electron with $m = \pm 1/2, 3/2, \dots$, the TAM of the final muon becomes

$$j_{4,z} = m - \lambda_2 - \lambda_3. \quad (132)$$

Dealing with the unpolarized initial muon and the final electron, the incoming electron TAM m is simply transferred to the muon,

$$\langle \hat{j}_z \rangle^{(\mu)} = m. \quad (133)$$

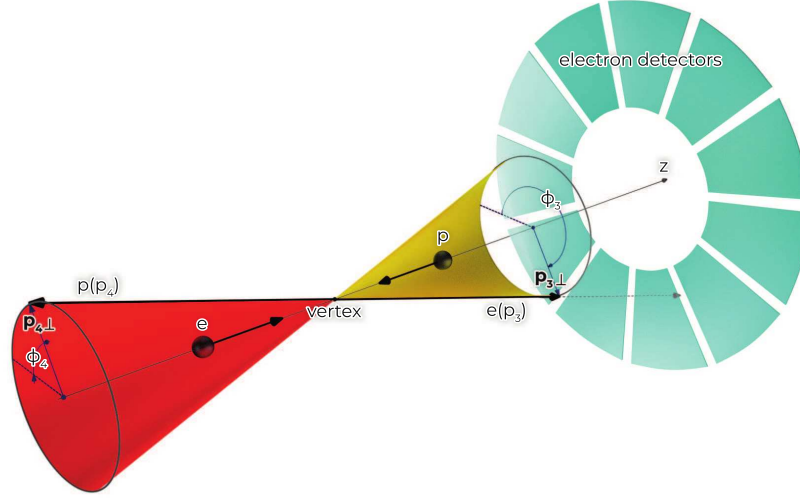


FIG. 7. An azimuthal “which-way” experiment with elastic $ep \rightarrow ep$ scattering. The evolved state of the proton becomes twisted if the electron azimuthal angle ϕ_3 is measured with a large error or not measured at all. The same scheme can also be applied to elastic and inelastic processes with other hadrons, ions, and nuclei.

Clearly, the same TAM-transfer can be realized in other processes like $e^-e^+ \leftrightarrow 2\gamma, e^-e^+ \rightarrow \tau^-\tau^+$, etc. It has been recently shown in Ref. [49] that a hallmark of the muon’s twisted state is the modification of the electron spectra as the incoming muon decays into an electron and two neutrinos. Such a modification can be experimentally observed, which would prove the vortex state of the muon.

B. Hadrons

Finally, we examine scattering off a hadron taking as an example elastic scattering of an electron by a proton with a mass m_p ,

$$e(p_1) + p(p_2) \rightarrow e(p_3) + p(p_4), \quad (134)$$

in the same head-on geometry (see Fig.7) with $p_3 = \{\varepsilon_3, p_{3,\perp} \cos \phi_3, p_{3,\perp} \sin \phi_3, p_{3,z}\}$ and similarly for p_4 . Generalization to other hadrons, ions, nuclei, or to the inelastic processes due to the non-electromagnetic forces (say, to deep-inelastic ep scattering) is straightforward.

The plane-wave matrix element is

$$S_{fi}^{(pw)} = i(2\pi)^4 N \delta^{(4)}(p_1 + p_2 - p_3 - p_4) \times \frac{4\pi e^2}{q^2} (\bar{u}_3 \gamma^\mu u_1) (\bar{u}_4 \Gamma_\mu u_2), \quad (135)$$

where

$$\Gamma_\mu = F_1 \gamma_\mu + F_2 \sigma_{\mu\nu} q^\nu \quad (136)$$

is a hadronic vertex, which is parametrized with two form-factors [68, 69]

$$F_1 = F_1(q^2, P^2), F_2 = F_2(q^2, P^2), \quad (137)$$

where

$$q^2 = (p_1 - p_3)^2, P^2 = (p_4 + p_2)^2/4 \quad (138)$$

do not depend on the angle ϕ_4 of the final proton. So the form-factors do not depend on it either. Here also

$$\sigma^{\mu\nu} = \frac{1}{2}(\gamma^\mu \gamma^\nu - \gamma^\nu \gamma^\mu) = (\boldsymbol{\alpha}, i\boldsymbol{\Sigma}), \quad (139)$$

where $\boldsymbol{\alpha}, \boldsymbol{\Sigma}$ are the 4×4 Dirac matrices in the standard representation [68].

Then, one can prove that

$$\bar{u}_3(\phi_3 = \phi_4 \pm \pi) \gamma^\mu u_1 (\bar{u}_4 \Gamma_\mu u_2) \propto e^{i(\lambda_1 - \lambda_2 - \lambda_3 - \lambda_4)\phi_4}. \quad (140)$$

Dealing with the 4-vector

$$\sigma^{\mu\nu} q_\nu = -\{\boldsymbol{\alpha} \cdot \mathbf{q}, \boldsymbol{\alpha} q_0 + i\boldsymbol{\Sigma} \times \mathbf{q}\}, \quad (141)$$

at the form-factor F_2 , we need to calculate the following averages (cf. with Eq.(49) and Eq.(53)):

$$\begin{aligned} \bar{u}_{p'\lambda'} \boldsymbol{\alpha} u_{p\lambda} &= (2\lambda\sqrt{\varepsilon - m_p}\sqrt{\varepsilon' + m_p} - 2\lambda'\sqrt{\varepsilon + m_p}\sqrt{\varepsilon' - m_p}) \\ &\quad \times 2\lambda \left(d_{\lambda\lambda'}^{(1/2)}(\theta') \chi_0 - \sqrt{2} d_{-\lambda\lambda'}^{(1/2)}(\theta') \chi_{2\lambda} e^{-2i\lambda\phi'} \right) e^{i(\lambda - \lambda')\phi'}, \\ \bar{u}_{p'\lambda'} \boldsymbol{\Sigma} u_{p\lambda} &= (\sqrt{\varepsilon + m_p}\sqrt{\varepsilon' + m_p} - 2\lambda 2\lambda'\sqrt{\varepsilon - m_p}\sqrt{\varepsilon' - m_p}) \\ &\quad \times 2\lambda \left(d_{\lambda\lambda'}^{(1/2)}(\theta') \chi_0 - \sqrt{2} d_{-\lambda\lambda'}^{(1/2)}(\theta') \chi_{2\lambda} e^{-2i\lambda\phi'} \right) e^{i(\lambda - \lambda')\phi'}, \end{aligned}$$

$$\begin{aligned}
\bar{u}_{p'\lambda'} \boldsymbol{\alpha} u_{p\lambda}(-\mathbf{p}) &= (2\lambda\sqrt{\varepsilon-m_p}\sqrt{\varepsilon'+m_p} - 2\lambda'\sqrt{\varepsilon+m_p}\sqrt{\varepsilon'-m_p}) \\
&\quad \times 2\lambda \left(-d_{-\lambda\lambda'}^{(1/2)}(\theta') \chi_0 + \sqrt{2} d_{\lambda\lambda'}^{(1/2)}(\theta') \chi_{-2\lambda} e^{2i\lambda\phi'} \right) e^{-i(\lambda+\lambda')\phi'}, \\
\bar{u}_{p'\lambda'} \boldsymbol{\Sigma} u_{p\lambda}(-\mathbf{p}) &= (\sqrt{\varepsilon+m_p}\sqrt{\varepsilon'+m_p} - 2\lambda 2\lambda'\sqrt{\varepsilon-m_p}\sqrt{\varepsilon'-m_p}) \\
&\quad \times 2\lambda \left(-d_{-\lambda\lambda'}^{(1/2)}(\theta') \chi_0 + \sqrt{2} d_{\lambda\lambda'}^{(1/2)}(\theta') \chi_{-2\lambda} e^{2i\lambda\phi'} \right) e^{-i(\lambda+\lambda')\phi'}.
\end{aligned} \tag{142}$$

Here, two former averages correspond to the proton moving along the z axis, whereas two latter ones are calculated for the proton moving opposite to this axis. We have also denoted for simplicity $\phi_4 \equiv \phi'$, $\lambda_4 \equiv \lambda'$, $\lambda \equiv \lambda_2$, $\theta_4 \equiv \theta'$.

The evolved wave function of the final proton is defined by Eq.(40),

$$\psi_p^{(f)} = \sum_{\lambda_4=\pm 1/2} \int_0^{2\pi} \frac{d\phi_3}{2\pi} u_4 S_{fi}^{(pw)} \tag{143}$$

Clearly, within the same generalized-measurement scheme (see Fig.7) the evolved wave function of the proton becomes twisted,

$$\hat{j}_{4,z} \psi_p^{(f)} = (\lambda_1 - \lambda_2 - \lambda_3) \psi_p^{(f)}. \tag{144}$$

When the incoming electron is twisted with the TAM z -projection m , we have

$$\lambda_1 - \lambda_2 - \lambda_3 \rightarrow m - \lambda_2 - \lambda_3 \tag{145}$$

If the initial hadron is unpolarized and the electron polarization is not measured, the electron TAM is transferred to the hadron,

$$\langle \hat{j}_z \rangle^{(p)} = m. \tag{146}$$

Clearly, this transfer can also be realized for other particles, regardless of their masses and spins, including neutrons, pions, atoms, ions, and nuclei.

VII. DISCUSSION AND CONCLUSION

We have theoretically demonstrated that the vortex states of particles of arbitrary mass, spin, and energy can be generated in a number of customary processes of photon emission, lepton and hadron scattering, or annihilation simply by abandoning the standard projective measurement protocol. The key condition that determines vorticity in the quantum theory is not the incoming particle trajectory, but the postselection with the generalized measurement of the azimuthal angle. Somewhat surprisingly, it is this scheme with the large measurement error that most adequately describes the emission of twisted photons when the recoil is very small, thus providing complete agreement with the classical theory in the spirit of the correspondence principle.

We have given explicit examples for the simplest case when the measurement error of the angle is maximized,

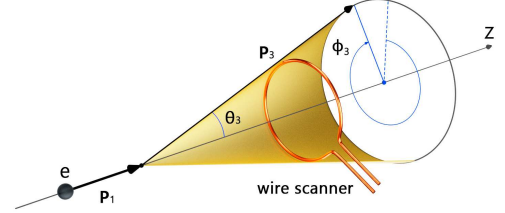


FIG. 8. A ring-shaped wire scanner detects electrons scattered at a certain polar angle, but does not measure the azimuthal angle.

$\sigma_\phi \rightarrow 2\pi$, and the resultant vortex states turn out to be the Bessel beams of photons, electrons, muons, hadrons, nuclei, etc. Were this error smaller, the resultant states would be the Bessel-like wave packets with a *finite uncertainty* of the angular momentum but with *the same central value*, defined by the TAM conservation law. In Fig.8 we show one of the simplest examples how one can detect an electron (a proton, an ion, or a nucleus) scattered at a certain polar angle, but deliberately do not get the information about its azimuthal angle.

The transverse momentum of the resultant twisted particle is defined by that of the other particle whose azimuthal angle is measured with a large error. Thus, selecting the particles scattered at larger polar angles – say, in $ep, \gamma e, \gamma p, \gamma$ -ion, or ion-ion collisions – one can obtain relativistic vortex beams with the desired transverse momentum. For instance, for hard X-ray or γ -range twisted photons obtained in collisions of intense laser pulses with GeV electrons or ions (say, at the Gamma Factory [6, 67]), the transverse momenta can reach the keV scale.

This method can readily be implemented for the production of highly energetic vortex particles at synchrotron radiation facilities and free-electron lasers with the helical undulators, such as the SASE3 undulator beamline of the European XFEL, at the powerful laser facilities aimed at studying the non-linear QED phenomena, such as, for instance, the Extreme Light Infrastructure, and at the existing and future lepton and hadron linear colliders.

ACKNOWLEDGMENTS

We are grateful to A. Di Piazza, A. Tishchenko, A. Surzhykov, A. Pupasov-Maksimov, and A. Volotka for fruitful discussions and criticism. The studies in Sec.II-IV are supported by the Russian Science Foundation (Project No. 21-42-04412) and by the Deutsche Forschungsgemeinschaft (Project No. SU 658/5-1). The studies in Sec.V are supported by the Ministry of Science and Higher Education of the Russian Federation (agreement No. 075-15-2021-1349). The studies in Sec.VI are supported by the Government of the Russian Federation through the ITMO Fellowship and Professorship Program.

Appendix A: OAM of a plane wave

A plane-wave state with a definite momentum \mathbf{p} and helicity λ can be expanded over cylindrical waves as follows:

$$|\mathbf{p}, \lambda\rangle = \sum_{\ell=-\infty}^{\infty} i^{\ell} e^{-i\ell\phi} |p_{\perp}, p_z, m = \ell + \lambda, \lambda\rangle. \quad (\text{A1})$$

The probability for the plane wave to have a definite OAM projection $\langle \hat{L}_z \rangle = \ell = 0, \pm 1, \pm 2, \dots$

$$|i^{\ell} e^{-i\ell\phi}|^2 = 1 \quad (\text{A2})$$

is independent of ℓ . This means that although the OAM mean value is vanishing for the plane wave, its OAM dispersion (or the OAM bandwidth) $\langle \hat{L}_z^2 \rangle$ is *infinitely wide*.

We can show it by explicit calculations. Let us first take the plane wave propagating strictly along the z axis with the momentum $\langle \mathbf{p} \rangle = \{0, 0, \langle p \rangle\}$ (we explicitly write \hbar in what follows),

$$e^{\frac{i}{\hbar} \langle \mathbf{p} \rangle \cdot \mathbf{r}} = e^{\frac{i}{\hbar} \langle p \rangle z}, \quad (\text{A3})$$

and so

$$\hat{L}_z e^{\frac{i}{\hbar} \langle \mathbf{p} \rangle \cdot \mathbf{r}} = \hat{L}_z^2 e^{\frac{i}{\hbar} \langle \mathbf{p} \rangle \cdot \mathbf{r}} = 0. \quad (\text{A4})$$

where

$$\hat{L}_z = -i\hbar \frac{\partial}{\partial \phi_r}. \quad (\text{A5})$$

Such a plane wave has a definite OAM in a sense that its OAM distribution $\langle \hat{L}_z^2 \rangle$ is vanishing together with the mean OAM value, while its azimuthal angle is undefined.

The situation is different if the wave does not propagate strictly along the z axis and has a transverse momentum p_{\perp} and a definite azimuthal angle ϕ_p ,

$$e^{\frac{i}{\hbar} \langle \mathbf{p} \rangle \cdot \mathbf{r}} = e^{\frac{i}{\hbar} p_{\perp} \rho \cos(\phi_p - \phi_r) + \frac{i}{\hbar} \langle p_z \rangle z}, \quad (\text{A6})$$

where

$$\langle \mathbf{p} \rangle = \{p_{\perp} \cos \phi_p, p_{\perp} \sin \phi_p, \langle p_z \rangle\},$$

$$\mathbf{r} = \{\rho \cos \phi_r, \rho \sin \phi_r, z\}. \quad (\text{A7})$$

Let us normalize the plane wave in a large cylinder with the volume $V = L\pi R^2$, so the mean value of an operator \hat{A} is

$$\langle \hat{A} \rangle = \frac{\int d^3r e^{-\frac{i}{\hbar} \langle \mathbf{p} \rangle \cdot \mathbf{r}} \hat{A} e^{\frac{i}{\hbar} \langle \mathbf{p} \rangle \cdot \mathbf{r}}}{V} = \frac{\int_{-L/2}^{L/2} dz \int_0^R d\rho \int_0^{2\pi} d\phi}{V} \hat{A}. \quad (\text{A8})$$

From here, we arrive at

$$\langle \hat{L}_z \rangle = 0, \quad \langle \hat{L}_z^2 \rangle = \frac{(p_{\perp} R)^2}{4} \rightarrow \infty, \text{ when } R \rightarrow \infty. \quad (\text{A9})$$

So, the definite azimuthal angle of the plane wave implies an infinitely wide OAM distribution with $\langle \hat{L}_z^2 \rangle \rightarrow \infty$ around the central value $\langle \hat{L}_z \rangle = 0$.

It is exactly the situation that we encounter in the scheme (i) of the projective measurements in the plane-wave basis in Sec.II C. Both final plane waves in a generic scattering, annihilation, or radiation process have non-vanishing transverse momenta, the definite azimuthal angles and, therefore, their mean OAMs are vanishing while the OAM dispersions are infinite.

Appendix B: Undulator radiation by a single electron in the quasi-classical regime

In classical electrodynamics within the paraxial approximation, the inhomogeneous wave equation for the slowly-varying amplitude of the electric field in the frequency domain $\tilde{\mathbf{E}}_{\perp}$ can be written as follows (the Gaussian units with $c = 1$ are used):

$$\mathcal{D} [\tilde{\mathbf{E}}_{\perp}(z, \mathbf{r}_{\perp}, \omega)] = \mathbf{g}_{\perp}(z, \mathbf{r}_{\perp}, \omega), \quad (\text{B1})$$

where the differential operator \mathcal{D} is defined by

$$\mathcal{D} \equiv \left(\nabla_{\perp}^2 + 2i\omega \frac{\partial}{\partial z} \right), \quad (\text{B2})$$

∇_{\perp}^2 being the Laplacian operator over transverse Cartesian coordinates. The source-term vector can be written in terms of the Fourier transform of the transverse current density, $\tilde{\mathbf{j}}_{\perp}(z, \mathbf{r}_{\perp}, \omega)$, and of the charge density, $\tilde{\rho}(z, \mathbf{r}_{\perp}, \omega)$ (both being macroscopic quantities treated as given), as

$$\mathbf{g}_{\perp} = -4\pi \exp[-i\omega z] (i\omega \tilde{\mathbf{j}}_{\perp} - \nabla_{\perp} \tilde{\rho}). \quad (\text{B3})$$

For a helical undulator, we set a constrained electron motion

$$\mathbf{r}_{o\perp}(z) = r_{ox} \mathbf{e}_x + r_{oy} \mathbf{e}_y \quad (\text{B4})$$

with

$$r_{ox}(z) = \frac{K}{\gamma_0 k_w} \cos(k_w z), \quad r_{oy}(z) = \frac{K}{\gamma_0 k_w} \sin(k_w z) \quad (\text{B5})$$

with the constant longitudinal speed along the z axis. Here

$$k_w = \frac{2\pi}{\lambda_w}, \quad K = \frac{eH_w}{k_w m_e}, \quad (\text{B6})$$

λ_w is an undulator period, and H_w is the maximal modulus of the undulator magnetic field on-axis. The classical parameter K is analogous to η from Eq.(87).

Solution of the wave equation is found to be:

$$\begin{aligned} \tilde{\mathbf{E}}_{\perp}(z, \mathbf{r}_{\perp}, \omega) = & \int_{-\infty}^z dz' \frac{1}{z-z'} \int d\mathbf{r}'_{\perp} \exp \left\{ i\omega \left[\frac{|\mathbf{r}_{\perp} - \mathbf{r}'_{\perp}|^2}{2(z-z')} \right] + i \left[\int_0^{z'} d\bar{z} \frac{\omega}{2\gamma_z^2(\bar{z})} \right] \right\} \\ & \times [(i\omega \mathbf{v}_{o\perp}(z') - \nabla'_{\perp}) \tilde{\rho}(z', \mathbf{r}'_{\perp} - \mathbf{r}_{o\perp}(z'), \omega)], \end{aligned} \quad (\text{B7})$$

Here $\gamma_z(z) = 1/\sqrt{1-v_{oz}(z)^2}$, and ∇'_{\perp} represents the gradient operator with respect to the source point, while (z, \mathbf{r}_{\perp}) indicates the observation point. The further calculations are very similar to those for a planar undulator presented in detail in Ref.[88].

Integration by parts of the gradient term, and introduction of a new integration variable $\mathbf{l} = \mathbf{r}'_{\perp} - \mathbf{r}_{o\perp}(z')$ gives the following expression in the far-zone limit for relativistic energies, $\gamma \gg 1$, and for the small emission angles $\theta_x = x/z \ll 1, \theta_y = y/z \ll 1$:

$$\begin{aligned} \tilde{\mathbf{E}}_{\perp}(z, \mathbf{r}_{\perp}, \omega) = & -\frac{i\omega}{z} \int d\mathbf{l} \int_{-\infty}^{\infty} dz' \tilde{\rho}(z', \mathbf{l}, \omega) \exp[i\Phi_T(z', \mathbf{l}, \omega)] \\ & \times \left[\left(\frac{K}{\gamma} \sin(k_w z') + \theta_x \right) \mathbf{e}_x + \left(-\frac{K}{\gamma} \cos(k_w z') + \theta_y \right) \mathbf{e}_y \right] \end{aligned} \quad (\text{B8})$$

where

$$\Phi_T = \omega \left\{ \frac{z'}{2\gamma^2} \left[1 + K^2 + \gamma^2 (\theta_x^2 + \theta_y^2) \right] - \right.$$

$$\left. - \frac{K\theta_x}{\gamma k_w} \cos(k_w z') - \frac{K\theta_y}{\gamma k_w} \sin(k_w z') \right\} + \Phi_0 \quad (\text{B9})$$

with $\Phi_0 = \omega [-(\theta_x l_x + \theta_y l_y) + \frac{z}{2} (\theta_x^2 + \theta_y^2)]$. Further use of the resonant approximation leads to

$$\begin{aligned} \tilde{\mathbf{E}}_{\perp s} = & \frac{K \omega_{s0}}{2\gamma z} \int_{-\infty}^{\infty} dl_x \int_{-\infty}^{\infty} dl_y \int_{-\infty}^{\infty} dz' \tilde{\rho}(z', \mathbf{l}, \omega) \exp[i\Phi_0] \exp \left\{ is \frac{\Delta\omega_s}{\omega_s} k_w z' \right\} \\ & \times \frac{1}{(s-1)!} \left(s \frac{K\gamma}{1+K^2} \right)^{s-1} (\theta_y - i\theta_x)^{s-1} (\mathbf{e}_x + i\mathbf{e}_y). \end{aligned} \quad (\text{B10})$$

where s is the harmonic number (cf. with Sec.V), $\omega = \omega_s + \Delta\omega_s$. A model for *the single-electron emission* is

obtained by setting

$$\tilde{\rho}(z, \mathbf{l}, \omega) = g_0(\mathbf{l}) \bar{f}(\omega), \quad (\text{B11})$$

for z in the range $(-L_w/2, L_w/2)$ and zero otherwise, L_w is the undulator length, and $g_0 = -e\delta(\mathbf{l})$ and $f(t) = \delta(t - t_e) \rightarrow f(\omega) = \exp(i\omega t_e)$. The direct substitution explicitly gives

$$\tilde{\mathbf{E}}_{\perp s} = -e \frac{K \omega}{2\gamma z} \exp \left[i \frac{\omega_{s0} z}{2} (\theta_x^2 + \theta_y^2) \right] L_w \text{sinc} \left[C_s L_w / z + (\theta_x^2 + \theta_y^2) \omega_{s0} L_w / (4) \right]$$

$$\frac{1}{(s-1)!} \left(s \frac{K\gamma}{1+K^2} \right)^{s-1} (\theta_y - i\theta_x)^{s-1} (\mathbf{e}_x + i\mathbf{e}_y). \quad (\text{B12})$$

where we have ignored the unimportant phase ωt_e . C_s is the so-called detuning parameter,

$$C_s = \frac{\omega}{2\bar{\gamma}_z^2} - s k_w = s \frac{\omega - \omega_{s0}}{\omega_{s0}} k_w, \\ \omega_{s0} = 2s k_w \bar{\gamma}_z^2, \quad \bar{\gamma}_z^2 = \frac{\gamma^2}{1+K^2}. \quad (\text{B13})$$

Finally, we note that $\mathbf{e}_x + i\mathbf{e}_y = -\sqrt{2}\boldsymbol{\chi}_{+1}$ with $\boldsymbol{\chi}_{+1}$ from Eq.(50). Going to cylindrical coordinates $\{\theta_x, \theta_y\} = \theta\{\cos\phi, \sin\phi\}$ and an infinitely long undulator, $L_w \rightarrow \infty$, we obtain in Eq.(B12) the same angular dependence and the same phase as for the non-linear Compton (or rather Thomson) scattering in the quasi-classical regime with the circularly polarized laser wave; see Eq.(117) in Sec.V B 2 where $\theta_{k'}, \phi_{k'}$ are analogous to θ, ϕ , respectively.

-
- [1] L. Allen, M. W. Beijersbergen, R. J. C. Spreeuw, and J. P. Woerdman, Orbital angular momentum of light and the transformation of Laguerre-Gaussian laser modes, *Phys. Rev. A* **45**, 8185 (1992).
- [2] J. P. Torres, L. Torner, Twisted Photons: Applications of Light With Orbital Angular Momentum. Wiley-Vch Verlag, John Wiley and Sons, Weinheim (2011).
- [3] D. L. Andrews, M. Babiker, The Angular Momentum of Light, Cambridge University Press, Cambridge (2012).
- [4] B. A. Knyazev, V. G. Serbo, Beams of photons with nonzero projections of orbital angular momenta: New results, *Phys. Usp.* **61**, 449 (2018).
- [5] F. Tamburini, Bo Thidé, G. Molina-Terriza, G. Anzolin, Twisting of light around rotating black holes, *Nat. Phys.* **7**, 195 (2011).
- [6] D. Budker, J. R. Crespo López-Urrutia, A. Derevianko, V. V. Flambaum, M. W. Krasny, A. Petrenko, S. Pustelny, A. Surzhykov, V. A. Yerokhin, and M. Zolotarev, Atomic physics studies at the Gamma Factory at CERN, *Ann. Phys. (Berlin)* **532**, 2000204 (2020).
- [7] Y. Taira, Y. Kohmura, Measuring the topological charge of an x-ray vortex using a triangular aperture, *J. Opt.* **21**, 045604 (2019).
- [8] I. Ivanov, Double-Twisted Spectroscopy with Delocalized Atoms, *Ann. Phys. (Berlin)* **2021**, 2100128 (2021).
- [9] I. P. Ivanov, B. Liu, P. Zhang, Observability of the superkick effect within a quantum-field-theoretical approach, *Phys. Rev. A*, **105**, 013522 (2022).
- [10] S. Sasaki, I. McNulty, R. Dejus, Undulator radiation carrying spin and orbital angular momentum, *Nuclear Instruments and Methods in Physics Research A* **582**, 43 (2007).
- [11] S. Sasaki, I. McNulty, Proposal for Generating Brilliant X-Ray Beams Carrying Orbital Angular Momentum, *Phys. Rev. Lett.* **100**, 124801 (2008).
- [12] A. Afanasev, A. Mikhailichenko, On Generation of Photons Carrying Orbital Angular Momentum in the Helical Undulator, arXiv:1109.1603 (2011).
- [13] J. Bahrtdt, K. Holldack, P. Kuske, R. Müller, M. Scheer, and P. Schmid, *Phys. Rev. Lett.* **111**, 034801 (2013).
- [14] O. V. Bogdanov, P. O. Kazinski, G. Yu. Lazarenko, Probability of radiation of twisted photons by classical currents, *Phys. Rev. A* **97**, 033837 (2018).
- [15] O. V. Bogdanov, P. O. Kazinski, G. Yu. Lazarenko, Semi-classical probability of radiation of twisted photons in the ultrarelativistic limit, *Phys. Rev. D* **99**, 116016 (2019).
- [16] U. D. Jentschura, V. G. Serbo, Generation of High-Energy Photons with Large Orbital Angular Momentum by Compton Backscattering, *Phys. Rev. Lett.* **106**, 013001 (2011).
- [17] U. D. Jentschura, V. G. Serbo, Compton upconversion of twisted photons: backscattering of particles with non-planar wave functions, *Eur. Phys. J. C* **71**, 1571 (2011).
- [18] Y. Taira, T. Hayakawa, M. Katoh, Gamma-ray vortices from nonlinear inverse Thomson scattering of circularly polarized light, *Scientific Reports* **7**, 5018 (2017).
- [19] M. Katoh, M. Fujimoto, N. S. Mirian, T. Konomi, Y. Taira, T. Kaneyasu, M. Hosaka, N. Yamamoto, A. Mochihashi, Y. Takashima, K. Kuroda, A. Miyamoto, K. Miyamoto, S. Sasaki, Helical Phase Structure of Radiation from an Electron in Circular Motion, *Scientific Reports* **7**, 6130 (2017).
- [20] M. Katoh, M. Fujimoto, H. Kawaguchi, K. Tsuchiya, K. Ohmi, T. Kaneyasu, Y. Taira, M. Hosaka, A. Mochihashi, and Y. Takashima, Angular Momentum of Twisted Radiation from an Electron in Spiral Motion, *Phys. Rev. Lett.* **118**, 094801 (2017).
- [21] V. Epp, U. Guselnikova, I. Kamenskaya, Angular momentum transferred by the field of a moving point charge, *Phys. Rev. A* **105**, 023511 (2022).
- [22] O. V. Bogdanov, P. O. Kazinski, G. Yu. Lazarenko, Proposal for experimental observation of the twisted photons in transition and Vavilov-Cherenkov radiations, *JINST* **15**, C04052 (2020).
- [23] O. V. Bogdanov, P. O. Kazinski, P. S. Korolev, G. Yu. Lazarenko, Radiation of twisted photons from charged particles moving in cholesterics, *Journal of Molecular Liquids* **326**, 115278 (2021).
- [24] D. V. Karlovets, V. G. Serbo, A. Surzhykov, Wave function of a photon produced in the resonant scattering of twisted light by relativistic ions, *Phys. Rev. A* **104**, 023101 (2021).
- [25] K. Yu. Bliokh, M. R. Dennis, and F. Nori, Relativistic Electron Vortex Beams: Angular Momentum and Spin-Orbit Interaction, *Phys. Rev. Lett.* **107**, 174802 (2011).
- [26] K. Y. Bliokh, I. P. Ivanov, G. Guzzinati, L. Clark, R. Van Boxem, A. Béchéd, R. Juchtmans, M. A. Alonso, P. Schattschneider, F. Nori, J. Verbeeck, Theory and ap-

- lications of free-electron vortex states, *Phys. Rep.* **690**, 1 (2017).
- [27] M. Uchida and A. Tonomura, Generation of electron beams carrying orbital angular momentum, *Nature* **464**, 737 (2010).
- [28] J. Verbeeck, H. Tian, P. Schlattschneider, Production and application of electron vortex beams, *Nature* **467**, 301 (2010).
- [29] B. J. McMorran A. Agrawal, I. M. Anderson, et al., Electron vortex beams with high quanta of orbital angular momentum, *Science* **331**, 192 (2011).
- [30] S. M. Lloyd, M. Babiker, G. Thirunavukkarasu, and J. Yuan, Electron vortices: Beams with orbital angular momentum, *Rev. Mod. Phys.* **89**, 035004 (2017).
- [31] I. P. Ivanov, Colliding particles carrying non-zero orbital angular momentum, *Phys. Rev. D* **83**, 093001 (2011).
- [32] I. P. Ivanov, V. G. Serbo, Scattering of twisted particles: Extension to wave packets and orbital helicity, *Phys. Rev. A* **84**, 033804 (2011).
- [33] D. V. Karlovets, Electron with orbital angular momentum in a strong laser wave, *Phys. Rev. A* **86**, 062102 (2012).
- [34] I. P. Ivanov, Creation of two vortex-entangled beams in a vortex-beam collision with a plane wave, *Phys. Rev. A* **85**, 033813 (2012).
- [35] I. P. Ivanov, Measuring the phase of the scattering amplitude with vortex beams, *Phys. Rev. D* **85**, 076001 (2012).
- [36] D. Seipt, A. Surzhykov, and S. Fritzsche, Structured x-ray beams from twisted electrons by inverse Compton scattering of laser light, *Phys. Rev. A* **90**, 012118 (2014).
- [37] V. G. Serbo, I. Ivanov, S. Fritzsche, D. Seipt, A. Surzhykov, Scattering of twisted relativistic electrons by atoms, *Phys. Rev. A* **92**, 012705, (2015).
- [38] I. Kaminer, M. Mutzafi, A. Levy, G. Harari, H. H. Sheinfux, S. Skirlo, J. Nemirovsky, J. D. Joannopoulos, M. Segev, and M. Soljačić, Quantum Čerenkov Radiation: Spectral Cutoffs and the Role of Spin and Orbital Angular Momentum, *Phys. Rev. X* **6**, 011006 (2016).
- [39] I. P. Ivanov, V. G. Serbo, and V. A. Zaytsev, Quantum calculation of the Vavilov-Cherenkov radiation by twisted electrons, *Phys. Rev. A* **93**, 053825 (2016).
- [40] I. P. Ivanov, D. Seipt, A. Surzhykov, S. Fritzsche, Elastic scattering of vortex electrons provides direct access to the Coulomb phase, *Phys. Rev. D* **94**, 076001 (2016).
- [41] D. V. Karlovets, Scattering of wave packets with phases, *J. High Energy Phys.* **03**, 049 (2017).
- [42] J. A. Sherwin, Compton scattering of Bessel light with large recoil parameter, *Phys. Rev. A* **96**, 062120 (2017).
- [43] J. A. Sherwin, Two-photon annihilation of twisted positrons, *Phys. Rev. A* **98**, 042108 (2018).
- [44] D. V. Karlovets, V. G. Serbo, Effects of the transverse coherence length in relativistic collisions, *Phys. Rev. D* **101**, 076009 (2020).
- [45] I. P. Ivanov, N. Korchagin, A. Pimikov, and P. Zhang, Doing spin physics with unpolarized particles, *Phys. Rev. Lett.* **124**, 192001 (2020).
- [46] I. P. Ivanov, N. Korchagin, A. Pimikov, and P. Zhang, Twisted particle collisions: a new tool for spin physics, *Phys. Rev. D* **101**, 096010 (2020).
- [47] I. P. Ivanov, N. Korchagin, A. Pimikov, and P. Zhang, Kinematic surprises in twisted-particle collisions, *Phys. Rev. D* **101**, 016007 (2020).
- [48] I. Madan, G. M. Vanacore, S. Gargiulo, T. LaGrange, and F. Carbone, The quantum future of microscopy: Wave function engineering of electrons, ions, and nuclei, *Appl. Phys. Lett.* **116**, 230502 (2020).
- [49] P. Zhao, I. P. Ivanov, P. Zhang, Decay of the vortex muon, *Phys. Rev. D* **104**, 036003 (2021).
- [50] A. V. Maiorova, A. V. Peshkov, A. A. Surzhykov, Radiative recombination of twisted electrons with hydrogenlike heavy ions: Linear polarization of emitted photons, *Phys. Rev. A* **104**, 022821 (2021).
- [51] I. P. Ivanov, Promises and challenges of high-energy vortex states collisions, *Progress in Particle and Nuclear Physics* (2022), in press; <https://doi.org/10.1016/j.ppnp.2022.103987>.
- [52] K. Floettmann, and D. Karlovets, Quantum mechanical formulation of the Busch theorem, *Phys. Rev. A* **102**, 043517 (2020).
- [53] D. Karlovets, Vortex particles in axially symmetric fields and applications of the quantum Busch theorem, *New J. Phys.* **23**, 033048 (2021).
- [54] A. Burov, S. Nagaitsev, Y. Derbenev, Circular modes, beam adapters, and their applications in beam optics, *Phys. Rev. E* **66**, 016503 (2002).
- [55] K.-J. Kim, Round-to-flat transformation of angular-momentum-dominated beams, *Phys. Rev. ST Accel. Beams* **6**, 104002 (2003).
- [56] Y.-E. Sun, P. Piot, K.-J. Kim, N. Barov, S. Lidia, J. Santucci, R. Tikhoplav, J. Wennerberg, Generation of angular-momentum-dominated electron beams from a photoinjector, *Phys. Rev. ST Accel. Beams* **7**, 123501 (2004).
- [57] C. Jia, D. Ma, A. F. Schäffer, J. Berakdar, Twisted magnon beams carrying orbital angular momentum, *Nature Comm.* **10**, 2077 (2019).
- [58] A. V. Afanasev, D. V. Karlovets, V. G. Serbo, Elastic scattering of twisted neutrons by nuclei, *Phys. Rev. C* **103**, 054612 (2021).
- [59] A. Luski, Y. Segev, R. David, O. Bitton, H. Nadler, A. R. Barnea, A. Gorlach, O. Cheshnovsky, I. Kaminer, E. Narevicius, Vortex beams of atoms and molecules, *Science* **373**, 1105 (2021).
- [60] A. Béché, R. van Boxem, G. van Tendeloo, J. Verbeeck, Magnetic monopole field exposed by electrons, *Nat. Phys.* **10**, 26 (2014).
- [61] Ch. W. Clark, R. Barankov, M. G. Huber, M. Arif, D. G. Cory, and D. A. Pushin, Controlling neutron orbital angular momentum, *Nature* **525**, 504 (2015).
- [62] C. Greenshields, R. L. Stamps, S. Franke-Arnold, Vacuum Faraday effect for electrons, *Phys. Rev. Lett.* **113**, 240404 (2014).
- [63] C. R. Greenshields, R. L. Stamps, S. Franke-Arnold, S. M. Barnett, Is the angular momentum of an electron conserved in a uniform magnetic field? *Phys. Rev. Lett.* **113**, 240404 (2014).
- [64] C. Greenshields, S. Franke-Arnold, R. L. Stamps, Parallel axis theorem for free-space electron wavefunctions, *New J. Phys.* **17** (2015) 093015.
- [65] A. A. Sokolov, I. M. Ternov, *Relativistic electron*, Nauka, Moscow, (1974) [in Russian] [Radiation from Relativistic Electrons, Edited by C. W. Kilmister, American Institute of Physics Translation Series, New York, (1986)].
- [66] D. V. Karlovets, S. S. Baturin, G. Geloni, G. K. Sizykh, and V. G. Serbo, Generation of vortex particles via generalized measurements, arXiv:2201.07997.
- [67] D. Budker, J. C. Berengut, V. V. Flambaum, M. Gorchtein, J. Jin, F. Karbstein, M. W. Krasny,

- Y. A. Litvinov, A. Pálffy, V. Pascalutsa, A. Petrenko, A. Surzhykov, P. G. Thirolf, M. Vanderhaeghen, H. A. Weidenmüller, V. Zelevinsky, Expanding Nuclear Physics Horizons with the Gamma Factory, arXiv:2106.06584 (2021).
- [68] V. B. Berestetskii, E. M. Lifshitz and L. P. Pitaevskii, *Quantum Electrodynamics*, Oxford: Pergamon, 1982.
- [69] M. E. Peskin, D. V. Schroeder, *An introduction to quantum field theory* (Westview Press, 1995).
- [70] S. M. Barnett, *Quantum information* (New York, Oxford University Press, 2009).
- [71] M. A. Al Khafaji, C. M. Cisowski, H. Jimbrown, S. Croke, S. Pádua, and S. Franke-Arnold, Single-shot characterization of vector beams by generalized measurements, *Optics Express* **30**, 22396 (2022).
- [72] P. Carruthers, M. M. Nieto, Phase and angle variables in quantum mechanics, *Rev. Mod. Phys.* **40**, 411 (1968).
- [73] S. Franke-Arnold, S. M. Barnett, E. Yao, J. Leach, J. Courtial, and M. Padgett, Uncertainty principle for angular position and angular momentum, *New J. Phys.* **6**, 103 (2004).
- [74] Y. Aharonov, D. Z. Albert, L. Vaidman, How the result of a measurement of a component of the spin of a spin-1/2 particle can turn out to be 100, *Phys. Rev. Lett.* **60**, 1351 (1988).
- [75] Y. Aharonov and D. Rohrlich, *Quantum Paradoxes: Quantum Theory for the Perplexed*, WILEY-VCH Verlag GmbH & Co. KGaA, Weinheim, 2005.
- [76] B. Tamir, E. Cohen, Introduction to Weak Measurements and Weak Values, *Quanta* **2**, 7 (2013).
- [77] Y. Aharonov, E. Cohen, A. C. Elitzur, Foundations and applications of weak quantum measurements, *Phys. Rev. A* **89**, 052105 (2014).
- [78] V. G. Bagrov, D. M. Gitman, and A. S. Pereira, Coherent and semiclassical states of a free particle, *Phys.-Usp.* **57**, 891 (2014).
- [79] V. I. Ritus, *J. Russ. Laser Res.* **6**, 497 (1985).
- [80] A. Di Piazza, C. Müller, K. Z. Hatsagortsyan, and C. H. Keitel, Extremely high-intensity laser interactions with fundamental quantum systems, *Rev. Mod. Phys.* **84**, 1177 (2012).
- [81] A. Fedotov, A. Ilderton, F. Karbstein, B. King, D. Seipt, H. Taya, G. Torgrimsson, Advances in QED with intense background fields, arXiv:2203.00019.
- [82] J. Gea-Banacloche, Quantum theory of the free-electron laser: Large gain, saturation, and photon statistics, *Phys. Rev. A* **31**, 1607 (1985).
- [83] T. Heinzl, A. Ilderton, and B. King, Classical and quantum particle dynamics in univariate background fields, *Phys. Rev. D* **94**, 065039 (2016).
- [84] A. Halavanau, D. Seipt, I. Lobach, T. Raubenheimer, S. Nagaitsev, Z. Huang, C. Pellegrini, Undulator radiation generated by a single electron, Proc. 10th Int. Particle Accelerator Conf. (IPAC'19), Melbourne, Australia, May 2019, pp. 1867-1870; doi:10.18429/JACoW-IPAC2019-TUPRB089.
- [85] L. D. Landau, E. M. Lifshitz, *The Classical Theory of Fields* (Oxford, Pergamon, 1975).
- [86] D. Yu. Ivanov, G. L. Kotkin, V. G. Serbo, Complete description of polarization effects in emission of a photon by an electron in the field of a strong laser wave, *Eur. Phys. J. C* **36**, 127 (2004).
- [87] D. A. Varshalovich, A. N. Moskalev, and V. K. Khersonskii, *Quantum Theory of Angular Momentum* (World Scientific, Singapore, 1988).
- [88] G. Geloni, V. Kocharyan, and E. Saldin, Theoretical computation of the polarization characteristics of an X-ray Free-Electron Laser with planar undulator, *Optics Comm.* **356**, 435 (2015).